Dynamics of Th1/Th17 Responses and Antimicrobial Pathways in Leprosy Skin Lesions

Priscila R. Andrade[1], Feiyang Ma[2], Jing Lu[2], Jaime de Anda[3], Ernest Y. Lee[3,4], George W. Agak[1], Craig J. Dobry[5], Bruno J. de Andrade Silva[1], Rosane M.B. Teles[1], Lilah A. Mansky[1], Jonathan Perrie[2], Dennis Montoya[2], Bryan D. Bryson[6,7], Johann E. Gudjonsson[5], Gerard C. L. Wong[3], Euzenir N. Sarno[8], Matteo Pellegrini[2], Robert L. Modlin[1,9*]

[1] Division of Dermatology, Department of Medicine, David Geffen School of Medicine, University of California, Los Angeles, Los Angeles, California, United States of America.

[2] Department of Molecular, Cell, and Developmental Biology, University of California, Los Angeles, Los Angeles, California, United States of America.

[3] Department of Bioengineering, University of California, Los Angeles, Los Angeles, California, United States of America.

[4]Department of Dermatology, University of California San Francisco, San Francisco, CA, United States of America.

[5] Department of Dermatology, University of Michigan, Ann Arbor, MI, United States of America.

[6] Broad Institute of MIT and Harvard, Cambridge, MA, United States of America.

[7] Department of Biological Engineering, MIT, Cambridge, MA, United States of America.

[8] Leprosy Laboratory, Oswaldo Cruz Foundation, Rio de Janeiro, Brazil.

[9] Department of Microbiology, Immunology and Molecular Genetics, University of California, Los Angeles, Los Angeles, California, United States of America.

*Corresponding Author: Robert L. Modlin

Address: UCLA 52-121 CHS, 10833 Le Conte Avenue, Los Angeles, California, USA

Telephone: (818) 288-2343

E-mail: rmodlin@mednet.ucla.edu

“The authors have declared that no conflict of interest exists.”

Abstract

Background: Reversal reactions (RR) in leprosy are acute immune episodes marked by inflammation and bacterial clearance, offering a model to study the dynamics of host responses to *Mycobacterium leprae*. These episodes are often severe and difficult to treat, frequently progressing to permanent disabilities. We aimed to characterize the immune mechanisms and identify antimicrobial effectors during RR.

Methods: We performed RNA sequencing on paired skin biopsy specimens from nine leprosy patients collected before and at RR diagnosis, followed by differential gene expression and functional analysis. A machine learning classifier was applied to predict membrane-permeabilizing proteins. Antimicrobial activity was assessed in *M. leprae*-infected macrophages and axenic cultures.

Results: In the paired pre-RR and RR biopsy specimens, a 64-gene antimicrobial response signature was upregulated during RR and correlated with reduced *M. leprae* burden. Predicted upstream regulators included IL-1β, TNF, IFN-γ and IL-17, indicating activation of both Th1 and Th17 pathways. A machine learning classifier identified 28 genes with predicted membrane-permeabilizing antimicrobial activity, including S100A8. Four proteins (S100A7, S100A8, CCL17, CCL19) demonstrated antimicrobial activity against *M. leprae* in vitro. Scanning electron microscopy revealed membrane damage in bacteria exposed to these proteins.

Conclusion: RR is associated with a robust antimicrobial gene program regulated by Th1/Th17 cytokines. We identified potentially novel host antimicrobial effectors that exhibit activity against *M. leprae*, suggesting potential strategies to bolster Th1/Th17 responses for combating intracellular mycobacterial infections.

Funding: NIH grants R01 AI022553, R01 AR040312, R01 AR073252, R01 AI166313, R01 AI169526, P50 AR080594, 4R37 AI052453-21 and NSF grant DMR2325840.

Introduction

Central to an effective host defense strategy against intracellular pathogens is the interaction of the innate and adaptative immune systems to mount a robust cell-mediated immune (CMI) response involving antimicrobial mechanisms. Leprosy provides a human disease model to investigate such mechanisms, as the clinical manifestations correlate with the immune response to the intracellular bacterium *Mycobacterium leprae* (1). The CMI response is strongest in individuals in the self-limiting tuberculoid pole (T-lep), as evidenced by the T-helper (Th) 1 cytokine profile production (2) and the vitamin D-dependent antimicrobial pathway induced by IFN-γ that can program macrophages to kill intracellular bacteria (3, 4). As a result, these patients exhibit few, often self-healing skin lesions, in which *M. leprae* bacilli are rarely found. Conversely, individuals with the progressive lepromatous pole (L-lep) are susceptible to disseminated infection, displaying numerous skin lesions loaded with bacilli due to ineffective CMI response, and instead showing high antibody titers, Th2 cytokine production (2), and phagocytic macrophages permissive to infection (3).

Leprosy patients can undergo acute inflammatory episodes known as reactions that ignite intense immune responses followed by severe outcomes. Type I reaction or reversal reaction (RR) consists of a series of dynamic changes to the patient immunological state that occur either spontaneously before, during or after chemotherapy, typically with a shift from the lepromatous pole towards the tuberculoid pole of the spectrum (5–7). RR presents clinically with the sudden appearance of new inflammatory skin lesions or the exacerbation of existing ones with the presence of erythema and edema, often associated with peripheral nerve impairment (6, 8). Histologically, RR skin lesions exhibit organized granulomas similar to those found in T-lep lesions with the presence of intercellular edema and epithelioid cell populations (8, 9). Patients exhibit enhanced CMI response to *M. leprae* antigens associated with the reduction or clearance of bacilli in their skin lesions (10, 11), the influx of T helper $CD4^+$ and cytotoxic $CD8^+$ T cell populations (12), a shift from the Th2 to a Th1 profile (10, 12, 13), plasticity from M2-like

to M1-like macrophages (3), as well as an increase in IFN-γ-induced genes and decrease in IFN-β-triggered responses including IL-10 production (3, 4, 8).

The initial host response against mycobacterial infection includes the triggering of the innate immune response involving antimicrobial mechanisms, pattern recognition receptor pathway activation (14, 15), vitamin D pathway induction (3, 16, 17), production of antimicrobial peptides (18–20), and initiation of autophagy (21, 22). This innate response also leads to the subsequent activation of the adaptive immune response that leads to CMI. An effective CMI response against mycobacteria is dependent on the T cell release of antimicrobial effector molecules as well as induction of antimicrobial effector mechanisms in infected macrophages. Th1 cell release of IFN-γ (4, 20, 21) can induce antimicrobial activity against *M. leprae* and *M. tuberculosis* in human macrophages via the vitamin D-dependent pathway that results in autophagy, phagosomal maturation, and production of the antimicrobial peptide cathelicidin (4, 21, 22). Human $CD8^+$ cytotoxic T cells expressing the cytotoxic granule proteins granzyme B, perforin, and granulysin have been linked to host defense in leprosy and tuberculosis (23, 24), with both granulysin and granzyme B having direct antimycobacterial activity (25, 26). In addition, Th17 cells can release IL-26, which has direct antimicrobial activity against *M. leprae* and *M. tuberculosis* (27–29).

Longitudinal studies of patients before and at the onset of RR have been conducted previously (9, 13, 30–35), mostly examining the immune response in the peripheral blood, with some examining a small number of genes or proteins in patient lesions. In this study, we sought to uncover the dynamics of innate and adaptive antimicrobial mechanisms at the site of disease by investigating the dynamic changes in the RR transcriptome in paired skin biopsy samples collected from patients before and at the onset of RR.

Results

Differential gene expression analysis shows the dynamic change in antimicrobial gene expression during RR.

To study the dynamic changes in immune response genes at the site of infection associated with the onset of CMI response in RR, we performed RNA-sequencing on paired skin biopsy specimens from nine leprosy patients obtained at the time of diagnosis with multibacillary disease (pre-RR) and at the clinical presentation of RR (RR) (Supplemental Figure 1). The inclusion of these patients in our study was supported by clinical examination and histopathologic correlation by experienced leprologists at the Oswaldo Cruz Foundation (Supplemental Figure 2)**.**

We isolated total RNA from eighteen skin specimens (n=9 pre-RR and n=9 RR) (Supplemental Table 1), depleted human ribosomal RNA to enrich the samples for mRNAs, prepared stranded libraries and submitted the samples for sequencing. Dimensionality reduction on the transcriptome data didn't show clear separation of the pre-RR and RR samples into distinct clusters, likely due to the shared characteristics of the paired individuals, as seen previously (34) (Supplemental Figure 3). To uncover differences between the RR and pre-RR transcriptomes, we conducted a paired differential gene expression analysis. We identified 404 genes (*padj*<0.3) that were differentially expressed between the RR vs. pre-RR groups, of which 200 genes ($log_2FC>0.5$, *padj*<0.3) were upregulated in RR, while 79 genes were downregulated ($log_2FC< -0.5$, *padj*<0.3) (Supplemental dataset 1). Hierarchical clustering analysis using the 404 differentially expressed genes showed segregation of the samples into two distinct clusters of nine samples each, one predominantly from pre-RR and the other from RR patients. The RR cluster contained one pre-RR sample, BL4, while the pre-RR cluster contained one RR sample, RR.BL6 (Figure 1A). BL4 and BL6 developed RR at 2.4 and 9.9 months after leprosy diagnosis, respectively (Supplemental Table 1). Histological review of all the biopsy specimens revealed that pairs BL4→RR.BL4 and BL6→RR.BL6 had the least pronounced differences between pre-

RR and RR states among all nine patients, providing one possible explanation for being outliers in the hierarchical clustering analysis.

A volcano plot of the differentially expressed genes revealed that the RR lesions highly expressed *CAMP*, *CYP27B1*, *VDR* and *IL1B*, elements of the vitamin D-dependent antimicrobial pathway (16, 19), as well as *IL26*, which encodes an antimicrobial protein released by IL-1β activated IL1R1^{+} Th17 cells (28, 36). RR specimens also expressed *S100A12*, which encodes an antimicrobial protein induced by TLR2/1L and IFN-γ in human macrophages (20), as well as *IL12B* and *IL12RB2*, known to be involved in host defense of leprosy (37). On the other hand, pre-RR lesions expressed genes that contribute to immunosuppression (*IL37*, *AIRE*) (38, 39) and genes involved in lipid metabolism or foamy macrophage biology (*DHRS3*, *SOAT2*, *CD5L, CD9, LEP*) (40–44) (Figure 1B).

Functional analysis of the RR upregulated gene signature using Metascape (45) showed significant enrichment for host defense pathways such as “Inflammatory response” ($-\log_{10}$*padj* =27.6), “Response to bacterium” ($-\log_{10}$*padj* =18.8), “IL-17 signaling pathway” ($-\log_{10}$*padj* =13.3) and “Chemotaxis” ($-\log_{10}$*padj* =11.7), reflecting the emergence of host defense mechanisms at the site of disease (Figure 2A). In addition, the RR pathways also included “Metal sequestration by antimicrobial proteins” ($-\log_{10}$*padj* = 10.1) and “Antimicrobial peptides” ($-\log_{10}$*padj* =7.8).

To elucidate the antimicrobial response in RR, we overlapped the RR upregulated 200-gene signature with a list of 1,693 genes encoding proteins involved in antimicrobial responses from the Gene Cards database, which identified a 64-gene antimicrobial response signature (enrichment $-\log_{10}$*p*-value = 15.9) (Supplemental dataset 2, Figure 2B and Supplemental Figure 4). A heatmap showing the expression of all 64 genes in the paired patient samples showed the dynamic upregulation of antimicrobial genes from pre-RR to RR (Figure 2C), despite the variable expression levels at the time of the pre-RR state. We calculated an antimicrobial response signature score by averaging the expression of all the 64 genes in each patient and then deriving z-scores. Our analysis showed a significant increase of the antimicrobial response

signature z-score in the RR group (mean=0.65, SEM±0.25) when compared to pre-RR specimens (mean= -0.65, SEM±0.27) (Figure 2D). Correlation analyses between each patient's antimicrobial response signature z-scores and clinical variables listed in Supplemental Table 1—including gender, age, multidrug therapy (MDT) duration, number of RR lesions, and time from leprosy diagnosis to RR onset—revealed no significant association between antimicrobial gene expression and these clinical features (data not shown). To validate the association of the 64-gene antimicrobial response signature in RR vs. pre-RR with the self-limiting vs. progressive forms, we mined other leprosy skin lesion RNA-seq data sets and signatures (Supplemental dataset 3). Overall, 48 of the 64-gene RR antimicrobial response signature were confirmed in the self-limiting forms (T-lep and RR) of other leprosy datasets.

Upstream regulator (UPR) analysis of the 64-gene antimicrobial response signature using Ingenuity Pathway Analysis (IPA) software, revealed that innate and adaptative immune cytokines were among the most significant upstream regulators, each targeting a high number of RR antimicrobial genes within the signature. Notable UPRs of this signature included *TNF* ($-\log_{10}$*padj* =47.1), *IL1B* ($-\log_{10}$*padj* =42.3), *IL17A* ($-\log_{10}$*padj* =38.5) and *IFNG* ($-\log_{10}$*padj* =24.8) (Figure 2E). The UPR analysis showed that 57 of the 64-gene antimicrobial response signature were regulated by these cytokines, with 44 RR antimicrobial genes (77.2%) being induced by either innate (*TNF* or *IL1B*) or adaptive cytokines (*IFNG* or *IL17A*). IL-1β and TNF were shown to exclusively induce the expression of 12 genes, while IFN-γ was the single inducer of only one antimicrobial gene in the signature (Supplemental Figure 5A). We mined an independent leprosy scRNA-seq dataset comprised of RR and L-lep skin lesions (GSE151528) (18) and determined that the main source of *IL1B* mRNA in RR skin lesions were myeloid cells, while *TNF* was expressed more by myeloid cells than T cells (Supplemental Figure 5B). *IFNG* expression was primarily detected in T cells with both *IFNG* and *TNF* predominantly expressed in the T-helper 17 (Th17) cells and RR cytolytic T lymphocytes (RR CTL) subpopulations (Supplemental Figure 5, C and D). *IL17A mRNA* was weakly expressed, however Th17 cells

have been detected in RR lesions by scRNA-seq (18, 46) based upon the key markers *RBPJ*, *RORA*, *RORC*, *IL23R* and *CCL20* (18) and IL-17 protein has been detected in T-lep skin lesions (47, 48).

We also determined the cells expressing the 64 antimicrobial response genes in the RR skin lesions, by calculating the average expression z-score of these genes in the scRNA-seq cell clusters identified in the RR and L-lep skin lesions (18). Of the 64 antimicrobial genes, 53 were found to have a z-score>2 in at least one cell subtype in the RR samples spanning myeloid cells, keratinocytes, endothelial cells, T cells and fibroblasts (Figure 3). *TNF*, one of the top UPRs of the RR antimicrobial response, regulated 54 of the 64 antimicrobial genes. Of these, 46 were detected in the leprosy single-cell RNA-seq dataset (18), with elevated expression (z-score > 2) observed in endothelial cells (n = 8), fibroblasts (n = 6), keratinocytes (n = 9), myeloid cells (n = 15), and T cells (n = 8), indicating a broad impact of *TNF* across multiple skin cell populations during RR. Similarly, among the 32 RR antimicrobial genes regulated by IL-17, 26 were identified in endothelial cells (n = 4), fibroblasts (n = 4), keratinocytes (n = 6), myeloid cells (n = 8), and T cells (n = 4). This widespread regulatory effect was also observed for IFN-γ and IL-1β, further supporting their role in shaping the RR skin lesion environment (Figure 3). Together our results indicate the contribution of both the innate and adaptive branches of the host immune response to the dynamic increase of the antimicrobial gene signature by different skin cell populations during the host response in RR, including the involvement of a robust Th17 helper response.

RR antimicrobial response gene signature is detected in T-lep patients and inversely correlates with M. leprae burden.

Our paired pre-RR and RR samples, by definition, included specimens from leprosy patients developing RR after the initiation of MDT. Since patients can spontaneously develop RR and present to the clinic prior to diagnosis and antibiotic treatment, we evaluated the

antimicrobial response in untreated patients across the spectrum of leprosy. To do so, we collected samples from the following patient groups: a RR group who developed the episode prior to MDT initiation (n=12) (RR pre-MDT group), a T-lep group composed of ten untreated borderline-tuberculoid (BT) patients, a BL group comprised of 6 BL from the pre-RR group and, a L-lep group composed of five untreated LL patients along with LL1 and LL2 from the original pre-RR group (Supplemental Table 2). An additional differential gene expression analysis between the original RR group vs. the new RR pre-MDT group showed that only eight genes were differentially expressed (*padj*<0.05) (*HTRA3*, *GFPT2*, *GNA14*, *MEDAG*, *OSMR*, *ANGPTL8*, *PLA2G2A* and *SLC39A14*) between these groups, suggesting that regardless of when the RR is triggered the episodes progress similarly. Dimension reduction analysis showed a clear separation of T-lep and L-lep samples (Supplemental Figure 6), while some of the RR pre-MDT and BL specimens were localized between the T-lep and L-lep groups or clustered with the T-lep group. Hierarchical clustering performed with the expression values of 64-gene antimicrobial response signature indicated co-clustering of most T-lep and RR pre-MDT samples due to the higher antimicrobial gene expression when compared to the BL and L-lep groups, which clustered together (Figure 4A). The RR pre-MDT samples RR6 and RR10 that clustered with the BL and L-lep groups were notable for the low expression of the 64-gene antimicrobial response signature, while the sample BL4 clustered with RR pre-MDT and T-lep groups.

To correlate the level of expression of the 64-gene antimicrobial response signature with clinical measures of bacillary load in leprosy patients that had not received MDT, we computed the z-score of the antimicrobial response signature in each patient. We observed a higher expression of the antimicrobial response signature z-score in T-lep (mean=0.53, SEM±0.25) and RR pre-MDT (mean=0.36, SEM±0.19) groups when compared to L-lep (mean= -0.93, SEM±0.22) individuals (Figure 4B). Although not significant, the BL group (mean = -0.53, SEM ± 0.56) exhibited lower average expression of the antimicrobial response signature z-score

compared to the T-lep and RR pre-MDT groups. We next examined the correlation of the antimicrobial gene expression with various measures of bacillary load, such as, *RLEP* (*M. leprae*-specific repetitive element) gene expression (49), skin bacillary index (SBI) and bacillary index (BI). In the groups without treatment, *RLEP* expression was positively correlated with the SBI values of the patients ($r= 0.87$, $p<0.0001$) (Supplemental Figure 7A) and inversely correlated with their 64-gene antimicrobial response signature z-scores (Figure 4C) ($r= -0.71$, $p<0.0001$). Furthermore, the 64-gene antimicrobial response signature z-scores inversely correlated with both the BI ($r= -0.62$, $p<0.0001$) and SBI ($r= -0.56$, $p=0.0005$) values (Supplemental Figure 7, B and C). We then conducted this analysis exclusively on the genes regulated by each UPR of the 64-gene antimicrobial response signature and observed that the individual antimicrobial gene programs induced by IL-17 (n= 32 genes), IFN-γ (n= 35 genes), TNF (n= 54 genes) and IL-1β (n= 44 genes) were also inversely correlated with the patient bacterial burden (Supplemental Figure 7, D-G). Taken together, these results indicate that the expression of the 64-gene antimicrobial response signature correlates with CMI and the host defense response against *M. leprae*.

Identification of molecules with direct antimicrobial activity in RR skin lesions.

We widened the scope of our RR transcriptome antimicrobial analysis by employing a machine learning-based membrane activity prediction tool (50) to identify sequences of antimicrobial proteins with predicted membrane-permeating properties or antimicrobial peptide (AMP)-like *motifs* within the 200 gene-RR upregulated signature. We evaluated the RR upregulated genes that encoded proteins known to be “antimicrobial”, “secreted” or located in the “extracellular matrix” according to the UNIPROT database annotation, restricting our analysis to 66 out the 200 RR genes (Supplemental dataset 4). We identified 41 RR upregulated genes that encoded proteins with AMP-like *motifs* (Figure 5A). These genes have known defined roles in innate and adaptive immune responses, comprising nine cytokines

(*IL1B*, *IL6*, *IL13*, *IL20*, *IL24*, *IL26*, *OSM*, *IL12B* and *CSF2*), five chemokines (*CCL1*, *CCL7*, *CCL17*, *CCL19* and *CCL22*), two growth factors (*NDP* and *PROK2*), four S100 proteins (*S100A7*, *S100A8*, *S100A12* and *S100A7A*), eight acute phase inflammatory molecules (*CP*, *LBP*, *LTF*, *PI3*, *PTX3*, *SAA2*, *CAMP* and *ORM1*), four enzymes (*LIPG*, *PLA2G2A*, *AKR1B10* and *SERPINE1*), one enzyme inhibitor (*TFPI2*), six tissue repair/remodeling proteins (*CHI3L1*, *CHI3L2*, *ADAMTS4*, *MMP1*, *MMP3*, *TNFAIP6*), one neural signaling molecule (*LGI2*) and one epidermal structural protein (*LCE3A*). Thirteen (*CAMP*, *CCL1*, *CCL17*, *CCL19*, *CCL22*, *IL26*, *LTF*, *PI3*, *PLA2G2A*, *S100A12*, *S100A7*, *S100A7A*, *SAA2*) of the 41 identified molecules were reported in the APD3 database (51) (Figure 5B), supporting the reliability of the machine learning classifier in predicting and identifying membrane-permeating peptide sequences. Despite having known antimicrobial activity, *KRT6A* and *RNASE2* were not included in the machine learning classifier analysis due to our initial selection criteria.

We cross-validated our machine learning classifier results against a previously reported AMP amino acid composition analysis known as the “saddle-splay” curve (52). The curve states an empirical relationship between the lysine-to-arginine ratio and mean hydrophobicity of a peptide to obtain antimicrobial membrane activity based on a dataset of 299 known AMPs. Our analysis confirmed that the AMP-like *motifs* within each of the 41 RR sequences exhibited comparable amino acid composition to the reference curve (Figure 5C). Hence, given the congruency between the two independent analyses, the identified AMP-like motifs may generate the topological negative gaussian curvature used by classical antimicrobial peptides to disrupt membranes rich in negative curvature lipids. The identification of 28 potentially novel antimicrobial protein candidates with membrane-permeating properties expressed in RR skin lesions, aside from the thirteen already known (51), gives further insight to the rich and complex host antimicrobial response that arises during leprosy’s RR.

Altogether, our analysis of genes encoding proteins with potential antimicrobial activity expressed in RR lesions identified 64 in the Gene Cards antimicrobial database and 41 with

predicted membrane permeating activity, in total comprising 77 unique genes (Supplemental dataset 5). Of these, fifteen genes were found in the direct antimicrobial peptide (APD3) data base (51): *CAMP*, *CCL1*, *CCL17*, *CCL19*, *CCL22*, *IL26*, *KRT6A*, *LTF*, *PI3*, *PLA2G2A*, *RNASE2*, *S100A12*, *S100A7*, *S100A7A*, *SAA2*. Twelve genes have been shown to participate in mycobacteria infection control, including *CAMP*, *IL26* and *CSF2* (Supplemental dataset 5). We further focused on the antimicrobial activity of four proteins that, to our knowledge, have not been shown to kill mycobacteria directly: CCL17, CCL19, S100A7 and S100A8. Of these, S100A8 is absent from the APD3 database (51), having been identified here as a membrane-permeating protein by the machine learning classifier.

Validation of S100A7, S100A8, CCL17 and CCL19 expression and antimicrobial activity against mycobacteria.

We first corroborated the gene expression in RR vs. pre-RR samples by qPCR (Supplemental Figure 8, A-D), showing a significant correlation with the RNA sequencing data (Supplemental Figure 8, E-H). Next, we validated the cell sources of these antimicrobial genes, previously determined by scRNA-seq (18), in the RR and pre-RR specimens by RNA *in situ* hybridization (RNA-FISH). We performed RNA-FISH on four paired skin lesions using specific mRNA probes along with probes or antibodies for specific cell population markers. Our results showed the presence of *S100A7* and *S100A8* mRNA in KRT14^{+} keratinocytes along the epidermis and in the hair follicles, more strongly expressed in RR vs. pre-RR lesions (Figure 6, A and B; Supplemental Figure 9). We confirmed expression of *CCL17* mRNA in myeloid cells by co-detection in lysozyme (*LYZ*) positive cells, representing activated macrophages (53), more highly expressed in the RR skin lesions (Figure 6C). The expression of *CCL19* mRNA in fibroblasts was validated in cells co-expressing type I collagen (*COL1A1*), more strongly detected in the dermis of RR vs. pre-RR skin lesions (Figure 6D). Negative and positive controls were performed for each skin lesion evaluated by RNA-FISH (Supplemental Figures 10 and 11).

We assessed the protein expression of S100A7, S100A8, CCL17 and CCL19 in RR vs. pre-RR skin lesions by immunohistochemistry (IHC). We observed that, in agreement with the scRNA-seq and RNA-FISH results, S100A7 and S100A8 were more expressed in RR skin lesions when compared to pre-RR specimens and their expression was concentrated on the epidermis (Figure 7A). S100A7 and S100A8 secretion by human keratinocyte cultures was also detected after stimulation with recombinant human IL-17, TNF or IFN-γ, upstream regulators of the RR antimicrobial gene signature (Supplemental Figure 12). Both CCL17 and CCL19 protein expression were also higher in RR skin lesions when compared to the pre-RR samples, with CCL17 present in the dermis in the same region as $CD68^{+}$ macrophages and CCL19 staining positive in cells scattered in the dermis and epidermis (Figure 7B).

We investigated the antimicrobial activity of S100A7, S100A8, CCL17 and CCL19 encoded proteins against *M. leprae* in human macrophages. We infected human monocyte-derived-macrophages (MDMs) with *M. leprae* at MOI 5:1, yielding an average infection rate of 75% of the cultured macrophages (Supplemental Figure 13). We added S100A7, S100A8, CCL17 and CCL19 (0.1μM) to the cultures and evaluated bacteria viability by qPCR after 4 days. Following titration assays, rifampin was selected as the positive control at a final concentration of 10 μg/mL (Supplemental Figure 14A). Our results showed that S100A7 (mean=99.2%, SEM±0.23), S100A8 (mean=97.4%, SEM±1.5), CCL17 (mean=87.7%, SEM±5.4) and CCL19 (mean=94.1%, SEM±3.0) exerted antimicrobial activity against *M. leprae* in cultured human macrophages, comparable to rifampin and notably higher than the ~40% reduction previously reported (27) for IL-26 at a higher concentration (2μM) (Figure 8, A-D).

The antimicrobial activity against *M. leprae* was abrogated by denaturation of the proteins prior to their addition to infected cultures (Supplemental Figure 14, B-E). Additional assays using leptin (0.1 μM) as a negative control showed no antimicrobial activity against *M. leprae*, indicating the specificity of S100A7, S100A8, CCL17, and CCL19 activity (Supplemental Figure 14F). Additionally, staining with viability dyes confirmed that these proteins did not impact

the viability of human macrophages (Supplemental Figure 15). Addition of S100A7, S100A8, CCL17 and CCL19 to MDMs infected with *Staphylococcus aureus* also led to the reduction of bacterial load in the macrophage cultures (Supplemental Figure 16A). Furthermore, in *M. leprae*-infected macrophages stimulated with S100A7, S100A8, CCL17 and CCL19, PKH26-labeled bacilli colocalized with Lysotracker staining, showing the bacteria in acidified phagolysosomes exhibiting signs of disintegration when compared to media control and negative control with 0.1μM of leptin (Figure 8E). These findings suggest that S100A7, S100A8, CCL17 and CCL19 lead to a reduction in *M. leprae* viability in infected macrophages.

Since these molecules interact with cell receptors to perform their classical functions, the antimicrobial activity observed in infected macrophages may have been indirectly triggered through receptor-ligand interactions. Therefore, to corroborate the machine learning classifier analysis, we tested the potential of S100A7, S100A8, CCL17 and CCL19 to directly kill mycobacteria by performing antimicrobial assays with *M. leprae* and *M. smegmatis* in axenic cultures. To conduct antimicrobial assays in axenic cultures, we performed dose titration experiments and found direct antimicrobial activity using recombinant human protein concentrations 10 to 200 times higher than those used in the *M. leprae*-infected macrophage assays. Our results indicated that S100A7, S100A8, CCL17 and CCL19 can significantly decrease the viability of *M. leprae* in axenic cultures, with the higher concentrations inducing antimicrobial activity comparable to that of rifampin (Figure 9, A-D). Similar experiments with auto-luminescent *Mycobacterium smegmatis* (54) and the mc(2)155 strain, showed that S100A7, S100A8, CCL17, and CCL19 exerted direct antimicrobial effects on these cultures (Supplemental Figure 17, A-H). Assays conducted in axenic cultures of *S. aureus* showed that S100A7, S100A8, CCL17, and CCL19 can also directly kill Gram-positive bacteria (Supplemental Figure 16, B-E).

We performed scanning electron microscopy to visualize the distinct morphological changes on the bacterial membranes of *M. leprae*, *M. smegmatis* and *S. aureus* after direct

exposure to S100A7, S100A8, CCL17 and CCL19. IL-26 was used as a positive control due to its direct antimicrobial activity against mycobacteria (27, 29). In the absence of antimicrobial proteins, *M. leprae* exhibited rod-shape morphology and intact cell surface at all time points, with a smoother membrane texture at 6h and 24h, and signs of corrugation at 48 and 96 hours, likely due to the bacteria's poor survival in axenic cultures. Conversely, membrane rupture and cytoplasmic leakage can be observed on the bacteria exposed to CCL17 and IL-26 as early as 6 hours, and to CCL19 as soon as 48 hours, with more pronounced damage observed in later time points. *M. leprae* bacilli exposed to S100A7 and S100A8 showed signs of severe surface wrinkling and roughening as early as 6 hours, with pronounced corrugation, but with no obvious signs of cytoplasmic leakage at the time points evaluated (Figure 9E).

Similar membrane alterations seen in *M. leprae* were also observed in *M. smegmatis* cultures after incubation with S100A8 for 6 hours, as well as with CCL17, CCL19 and IL-26 for 24 hours. In contrast, incubation of *M. smegmatis* with S100A7 for 6 hours revealed signs of membrane rupture and cytoplasmic leakage, which were not present at any time point in the *M. leprae* assay with S100A7 (Supplemental Figure 17I). Scanning electron microscopy images of *S. aureus* axenic cultures after exposure to S100A7, S100A8, CCL17 and CCL19 for 3 hours revealed membrane rupture and cytoplasmic leakage associated with antimicrobial activity (Supplemental Figure 16F). Taken together, our results suggest that these antimicrobial molecules contribute to host defense during *M. leprae* infection, either by targeting infected macrophages or by directly interacting with the bacilli during RR.

Discussion

Antimicrobial effector mechanisms, crucial components of both innate and adaptive immunity, play a vital role in combating intracellular bacterial infections, including *Mycobacterium leprae*, the etiologic agent of leprosy. The disease presents as a spectrum of clinical manifestations that correlate with the immune response, yet this spectrum is also dynamic, as patients may undergo RR. In this study, we conducted a longitudinal analysis of dynamic changes in the host transcriptome in lesions harvested from patients before and during RR, identifying 77 antimicrobial genes upregulated in RR. Our findings reveal the dynamic emergence of an antimicrobial gene program during RR as part of the host immune response, correlating with the reduction of bacterial burden in patients.

The development of reversal reactions in multibacillary leprosy patients marks a transition from a permissive immune environment that facilitates bacterial persistence to a state of enhanced cell-mediated immunity (13), often associated with a decline in the bacteriological index (10, 11, 55). The longitudinal design of our study enabled us to assess the dynamic emergence of host innate and adaptive immune response required to combat the infection, effectively controlling for individual variability, as each participant served as their own control. We identified a signature of 200 genes upregulated in RR vs. pre-RR skin lesions involved in innate and adaptive pathways contributing to CMI such as “Response to type II interferon” and “positive regulation of IL-12 production”, of which 64 are implicated in antimicrobial responses according to the Gene Cards database, including 12 with known antimicrobial roles in mycobacterial infection. An upstream regulator analysis of the 64-gene antimicrobial response signature showed the involvement of both innate (*TNF* and *IL1B*) and adaptative (*IL17A* and *IFNG*) cytokines in the induction of these antimicrobial genes. Strikingly, *IL17A* was identified as an upstream regulator for 32 of the 64 genes comprising the antimicrobial response signature. Th17 cells comprise 90% of the T cell population detected in RR skin lesions (18). In addition to confirming the role of *IFNG* and *IL1B* as regulators of antimicrobial gene expression in RR (18),

our data identified Th17 cells as the main source of *IFNG* and also secondarily contributing to *TNF* expression in RR skin lesions.

The identification of Th17 cells as major inducers of antimicrobial genes in RR lesions through the expression of *TNF*, *IFNG* and *IL17A* provides important new insights into the role of this T cell subset in leprosy immunopathogenesis. The IL17-induced antimicrobial gene program correlated with the reduction in viable bacilli in leprosy lesions. Previous studies have established the presence of Th17 cells in leprosy patients, in both RR (18) and T-lep skin lesions (47, 48, 56), as well as PBMCs of RR (56–58). Higher levels of IL-17 isoforms were detected in the resistant forms of leprosy (48, 59), including RR (60–62). Here, we found an IL-17-induced antimicrobial gene program with the potential to contribute to host defense in leprosy by encoding proteins with direct antimicrobial activity, as well as having pro-inflammatory properties that enhance the host response. In tuberculosis, caused by *M. tuberculosis*, Th17 cells have been shown to contribute to protective immunity, particularly in the early stages of infection (63) by playing a role in the induction of chemokines (64), recruitment of $CD4^+$ T cells (64) to the site of infection and formation of granulomas (65, 66). Altogether, our data further support the concept that RR involves coordinated interactions between the innate and adaptive immune systems, where bacterial ligands activate innate antigen-presenting cells that, in turn, prime the adaptive T cell response.

In addition to mining a literature-based database containing genes involved in antimicrobial responses, we also used a machine learning algorithm to predict proteins with direct antimicrobial activity. This prediction was based on the observation that antimicrobial peptides must generate a negative Gaussian curvature (NGC) to generate a membrane-permeating activity (52, 67). A total of 41 genes upregulated in RR skin lesions encoded proteins with predicted membrane-permeating properties. Of these, 13 have demonstrated direct antimicrobial activity against one or more pathogens from a broad spectrum tested (51). Of the other 28 genes, we further investigated S100A8, which forms a heterodimer with

S100A9, called calprotectin, with a broad spectrum of direct antimicrobial activity (68–73), although neither protein by itself has been shown to be directly antimicrobial. We determined that S100A8, along with three additional proteins encoded from the 77 unique antimicrobial genes (CCL17, CCL19 and S100A7), had direct antimicrobial activity against *M. leprae, M. smegmatis* and *S. aureus* in axenic cultures. By scanning electron microscopy, CCL17 and CCL19 induced bacterial membrane lysis with extrusion of cytoplasmic contents in all bacteria tested, as observed for IL-26 (28, 29) and other chemokines (74–76). S100A8 and S100A7 caused the extrusion of cytoplasmic contents in *S. aureus* and only surface wrinkling and corrugation in *M. leprae*. Given that S100 proteins can also contribute to antimicrobial responses by metal chelation (72, 73, 77), further studies are required to investigate the mechanism(s) of their antimicrobial activity against *M. leprae*. Thus, the approaches employed here led to the identification of four proteins that, to our knowledge, exhibited previously unreported direct antimicrobial activity against *M. leprae*.

In addition to having direct antibacterial activity, antimicrobial peptides can activate macrophages to kill intracellular bacteria. We found that S100A7, S100A8, CCL17 and CCL19 significantly reduced *M. leprae* viability within cultured human macrophages, demonstrating antimicrobial effects on infected cells that were comparable to those of rifampin. To our knowledge, only S100A8 has been reported to trigger an antimicrobial response in macrophages infected by mycobacteria, such as *M. tuberculosis and Mycobacterium bovis* (78, 79). The addition of antimicrobial peptides to macrophage cultures may lead to cell activation. For instance, S100A7 and S100A8 can mediate many of their biological functions through the pattern recognition receptor for advanced glycation end-products (RAGE), as well as TLR4 (80–83), leading to activation of NF-κB pathway, autophagy, and reactive oxygen species (ROS) production, mechanisms known to be involved in bacterial infection control (84–90). As has been shown for IL-26, these antimicrobial peptides are positively charged and could therefore

bind to DNA from dying cells (28), gain entrance to intracellular compartments and activate the stimulator of IFN genes (STING) pathway, inducing autophagy (27).

While our findings provide valuable insights into host defense mechanisms in RR skin lesions, we acknowledge some limitations of our study. Our antimicrobial assays were conducted in axenic cultures using micromolar concentrations of recombinant human proteins, a standard experimental approach (23, 27–29, 74, 75). However, physiological levels of S100A7 (91), S100A8 (92), CCL17 (93) and CCL19 (94) are typically in the pico- to nanomolar range. This discrepancy may partly reflect the use of recombinant proteins, which often lack native post-translational modifications and may exhibit misfolding, thereby reducing their functional activity (28, 95, 96). As mentioned previously, lower concentrations of antimicrobial peptides were required for antimicrobial activity against *M. leprae* in infected macrophages suggesting that cell activation potentiates the antimicrobial response. It is also important to note that our assays employed the *M. leprae* strain Thai-53 (genotype 1A), whereas the predominant strains in Brazil, where our cohort originates, are genotypes 3I and 4N (97) which may affect host responses (98). A future direction would be to perform strain-level sequencing (99, 100) to determine if there is a correlation with the host defense response. Finally, our human subject institutional review board limited the sampling from leprosy patients such that we used macrophages derived from healthy donor monocytes (3, 4, 20, 27), rather than from leprosy patients and limited tissue collection to a single skin biopsy per time point per patient.

The development of RR indicates the plasticity of both the innate and adaptive immune responses, dynamically switching from M2 to M1 macrophage phenotypes (3) and from Th2 to Th1 cytokine profiles (2), respectively, as well as from a bacterial persistence state towards the induction of antimicrobial response programs (3, 4). Our study offers a unique perspective of the dynamic CMI response during RR, uncovering potentially new host defense mechanisms against intracellular bacteria and expanding our understanding of antimicrobial programs that may contribute to future therapeutic approaches targeting intracellular mycobacterial infection.

Methods

Sex as a biological variable

Our study examined male and female patients and similar findings are reported for both sexes.

Leprosy biopsy specimens

Forty-five skin biopsy specimens were collected from leprosy patients classified by the Ridley & Jopling criteria (1966) (1) at the Souza Araújo Outpatient Unit (Oswaldo Cruz Foundation, Rio de Janeiro, Brazil) and snap frozen in liquid nitrogen using cryogenic tubes for later sectioning and RNA extraction. A single skin lesion was collected from each patient at each time point. Clinical diagnoses were confirmed through histopathology (H&E-stained sections) and acid-fast bacilli (AFB) staining. The pre-RR group (n=9) included six borderline-lepromatous (BL), one borderline-borderline (BB), and two lepromatous-lepromatous (LL) biopsies collected at diagnosis, before multidrug therapy (MDT). After sample collection, patients in the pre-RR group were prescribed a 12-month course of multidrug therapy (MDT), in accordance with the World Health Organization (WHO) guidelines. The RR group (n=9) consisted of biopsies from the same patients at RR diagnosis, before prednisone treatment. Eight RR samples were taken during MDT while sample RR.BL2 was collected approximately 10 months after MDT completion (Supplemental Table 1). The average time from leprosy diagnosis (LD) to RR onset among the nine patients was 8.5 months (SEM±2.05).

The T-lep group (n=10) included borderline-tuberculoid (BT) biopsies collected at diagnosis, prior to MDT. The L-lep group (n=7) included lepromatous-lepromatous (LL) lesions collected at diagnosis, also before MDT, with two specimens (LL1 and LL2) from the pre-RR group. The RR pre-MDT group (n=12) included RR cases diagnosed simultaneously with leprosy, without prior treatment for either condition (Supplemental Table 2). Finally, the BL group was comprised of six BL samples from the pre-RR group.

RNA sequencing of leprosy skin specimens

Frozen leprosy skin biopsies were sectioned (4 µm, 40 sections) and lysed in RLT Buffer (Qiagen, #79216) with 1% β-mercaptoethanol, then stored at -80°C. RNA extraction and library preparation were conducted as previously described (101). Ribosomal RNA depletion and library preparation were performed with Ribozero Gold (Illumina, #MRZG126) and KAPA Stranded RNA-Seq (Kapa Biosystems, #KR0934) kits. Libraries were quality-checked (Qubit, Bioanalyzer), barcoded, multiplexed (8 samples/lane, 10 µM/library), and sequenced on a HiSeq 4000 (Illumina, 100 bp single-end reads).

RNA sequencing data analysis

Sequenced reads were demultiplexed and aligned to the human genome (hg19, UCSC) using TopHat (v2.0.6) and Bowtie2 (v2.0.2), as previously described (102). Raw counts were generated with HTSeq and normalized using DESeq2. Dimensionality reduction of leprosy transcriptome data was performed with t-SNE on normalized counts of the most variable genes expressed in at least one sample, using the R package “tsne.” Differential gene expression between RR and pre-RR samples was analyzed using the paired inverted beta binomial test (R package “countdata”) (103). RR upregulated genes were identified as those with *padj*<0.3 and $\log_2$Fold-Change>0.5, while downregulated genes had *padj*<0.3 and $\log_2$Fold-Change< -0.5.

Functional gene analysis

Enrichment analysis of gene ontology (GO) terms, WikiPathways and Reactome gene sets was performed on the genes upregulated in RR vs. pre-RR groups using Metascape v3.5 (https://metascape.org/gp/index.html#/main/step1) (45).

RR antimicrobial response gene signature analysis

The RR antimicrobial response signature was derived from the overlap of upregulated genes in RR with a Gene Cards list of 1,693 molecules involved in antimicrobial responses and host defense (https://www.genecards.org/Search/Keyword?queryString=”antimicrobial”) (February 2023). Upstream regulator analysis (UPR) of this signature was performed using

Ingenuity Pathways Analysis (IPA-Qiagen). The antimicrobial response gene signature score for each patient was calculated as the mean expression of genes in the signature using $\log_{10}$ normalized counts. Z-scores were computed by subtracting the mean score and dividing by the standard deviation. Additionally, a list of human antimicrobial peptides (AMP) from the APD3 database (March 2023) (https://aps.unmc.edu/) was used to identify genes encoding proteins with direct antimicrobial activity (51).

M. leprae bacillary load indices

M. leprae burden of the leprosy specimens was evaluated by the bacillary index (BI) and skin bacillary index (SBI), which were generated by quantification of AFB in skin slit smears obtained from earlobes and in skin lesion sections by Wade Fite staining, respectively, using a logarithmic scale (104, 105). Relative bacterial burden in leprosy skin lesions was also determined by quantitative real-time PCR (qPCR) of *M. leprae* repetitive element (*RLEP*) DNA (49).

Cell population analysis using leprosy single cell RNA sequencing

We explored the cell population source of the RR antimicrobial response signature and their UPRs by mining a previous scRNA-seq data set (GSE151528) of untreated RR (n=5) and multibacillary skin lesions (n=5) (18). The major cell types including T cells, myeloid cells, keratinocytes, endothelial cells, and fibroblasts were found in both groups and z-scores using the average expression of genes across identified cell clusters were calculated, as previously described (18). A cut-off z-score>2 was applied to observe the specific RR antimicrobial genes for each cell type in the RR skin lesions.

Machine learning-based membrane activity prediction classifier

A machine-learning based membrane activity prediction classifier was used to discover amino acid sequences with membrane-permeating antimicrobial activity, or antimicrobial peptide (AMP)-like *motifs,* in the RR gene signature as previously described (50, 106, 107). The genes of the RR upregulated transcriptome were searched in the UNIPROT protein database

(https://www.uniprot.org/) by gene symbol and only the encoded proteins with the annotation keywords “secreted”, “extracellular matrix”, or “antimicrobial” were considered in the analysis. A candidate AMP-like gene encoding protein was considered for further evaluation if its median σ-score of its motifs was greater than 0.113 (or P(+1)>0.6) (Supplemental Methods).

Amino acid composition analysis of antimicrobial peptides

We applied the “saddle-splay selection rule” to further evaluate the amino acid sequence of the RR upregulated molecules unveiled by the machine learning classifier (52). We compared the amino acid composition of the RR upregulated protein encoding genes identified by the machine learning classifier to the compositions of a set of 299 known cationic antimicrobial peptide sequences obtained from the APD3 database (51). We calculated the mean hydrophobicity and the lysine (*K*) -to-arginine (*R*) ratio $N_K/(N_K + N_R)$ for each amino acid sequence. Only the amino acid composition of the predicted AMP-like motifs was used to compute such properties and for evaluation against the reference ”saddle-splay curve” (Supplemental Methods).

RNA fluorescence *in situ* hybridization (RNA-FISH)

RNA fluorescence in situ hybridization was performed on pre-RR and RR skin lesions using the RNAscope® Multiplex Fluorescent Detection Kit v2 (ACDBio, cat n°323100) following the manufacturer’s instructions. We used probes for *S100A7* (ACDBio-C2, cat n° 817121-C2), *S100A8* (ACDBio-C1, cat n°425271), *CCL17* (ACDBio-C1 cat n°468531), *CCL19* (ACDBio-C3, cat n°474361-C3), *COL1A1* (ACDBio-C2, cat n°401891-C2) and *LYZ* (ACDBio-C3, cat n°421441-C3) mRNA molecules. The RNAscope® 3-plex Positive Control Probe (cat n°320861) and the RNAscope® 3-plex Negative Control Probe (cat n°320871) were used as controls. Signal was detected using TSA™ Cyanine 3 & 5, TMR, Fluorescein Evaluation kit (PerkinElmer, cat n°NEL760001KT).

Identification of keratinocyte populations by immunofluorescence was performed as previously described (20, 27), with a cytokeratin 14 (KRT14) monoclonal antibody

(ThermoFisher scientific, cat n°MA5-11599, clone LL002) used at 2µg/ml. Quantification analysis was performed using Image J (Analyze Particles) on all pairs of RR and pre-RR skin lesions evaluated. Images were acquired with the Leica TCS SP8 Digital Light Sheet microscope.

Immunohistochemistry

Immunohistochemistry was performed as previously described (20, 27). Monoclonal antibodies (10µg/ml) for human S100A7 (ThermoFisher scientific, cat n°MA5-16199, clone 47c1068), S100A8 (R&D Systems, cat n°MAB4570, clone 749916), CCL19 (ThermoFisher scientific, cat n°MA5-23833, clone 54909), CCL17 (LSBio, cat n°LS-C198166, clone 1F11) and CD68 (2µg/ml) (Dako, cat n°M087629-2, clone PG-M1) were used. Monoclonal mouse IgG1 and IgG2b isotype controls (10µg/ml) were included in every assay. Staining was visualized using a Leica microscope (Leica 250) and protein expression was quantified using the Image J plugin ImmunoRatio (108).

Monocyte-derived Macrophages (MDMs)

PBMCs were isolated from peripheral blood using a Ficoll-hypaque (GE Healthcare) density gradient. MDMs were generated as previously described (20). Cells were maintained at 37°C with 5% CO_2.

Mycobacterium leprae

Live *M. leprae* (unlabeled or labeled with PKH26) was graciously provided by Dr. Ramanuj Lahiri of the National Hansen's Disease Program, Health Resources Service Administration, Baton Rouge, Louisiana. *M. leprae* was grown in athymic (nu/nu) mouse foot pad as previously described (109). All experiments with live *M. leprae* were performed at 35°C with 5% CO_2.

Antimicrobial assays with *M. leprae*-infected MDMs

Antimicrobial experiments with *M leprae*-infected MDMs were performed as previously described (20). Briefly, MDMs ($5x10^5$) were infected with *M. leprae* at a MOI of 5:1 overnight in

RPMI 1640 supplemented with 10% FCS without antibiotics at 35°C with 5% CO_2. Cells were stimulated the next day with 0.1µM of recombinant human S100A7 (R&D Systems, cat n°9085SA050), S100A8 (Biolegend, cat n°719906), CCL17 (Peprotech, cat n°300-30) and CCL19 (Peprotech, cat n°300-29B). Rifampin was added as a positive control (10µg/ml). Denatured recombinant proteins (0.1µM) and recombinant human leptin (Peprotech, cat n°300-27) were used as negative controls. After 4 days, TRIzol reagent was added to the cells. RNA and DNA extraction was performed according to the manufacturer's instructions. The viability of *M. leprae* was determined by qPCR (20, 27, 49). After $2^{-(\Delta Ct)}$ method analysis, the ratio of *16S* to *RLEP* was calculated and the percentage of bacterial viability was assessed relative to the media control.

Antimicrobial assays in axenic culture

For direct antimicrobial experiments with *M. leprae*, we added different concentrations of S100A7, S100A8, CCL19 and CCL17 to $2x10^6$ bacilli in Middlebrook 7H9 culture media supplemented with 10mM sodium phosphate dibasic (pH 7.2). Rifampin was used as a positive control (10µg/ml). *M. leprae* assays were performed for 3 days at 35°C. TRIzol was added to the pelleted bacteria and viability was assessed by qPCR as previously described (20, 27, 49). The ratio of *16S* to *RLEP* was calculated and the percentage of antimicrobial activity was calculated relative to the control.

Scanning Electron Microscopy

Scanning electron microcopy was performed as previously described (110). *M. leprae* ($15x10^6$), *M. smegmatis* ($5x10^6$) and *S. aureus* ($5x10^6$) antimicrobial assays were conducted in axenic culture with different incubation times. *M. leprae* assays were incubated for 6, 24, 48 and 96 hours at 35°C. *M. smegmatis* assays were incubated for 6 or 24 hours, and *S. aureus* assays were incubated for 3 hours at 37°C. Recombinant human IL-26 (R&D Systems, cat n° 1375-IL/CF-MTO) (10µM) was used as a positive control. Images were captured using a Zeiss Supra

40VP Field Emission Scanning Electron Microscope at an acceleration voltage of 10kV (Supplemental Methods).

Statistical analysis

Descriptive statistics for continuous variables were expressed as mean ± SEM. Data distribution was assessed using the Kolmogorov-Smirnov test with Dallal-Wilkinson-Lilliefor P value and/or Q-Q plots. Two groups of paired samples were compared using the ratio paired t test or paired t test, while independent groups were analyzed with one-way ANOVA followed by Tukey's or Dunnett's multiple comparisons test. Correlation analyses used Spearman's or Pearson's coefficients, depending on data distribution. For paired samples across multiple groups, we applied the Friedman test with Dunn's multiple comparisons test (non-normal data) or repeated measures ANOVA with Dunnett's multiple comparisons test (Gaussian data). Enrichment analysis of the RR transcriptome with the Gene Cards antimicrobial list was conducted using the hypergeometric distribution. Statistical analyses were performed in GraphPad Prism 9.12, with all tests (except hypergeometric) two-sided and significance set at $p<0.05$.

Study Approval

Human peripheral blood was obtained from healthy donors with informed consent (UCLA Institutional Review Board #11-001274). Leprosy skin specimens were obtained from the leprosy laboratory at the Oswaldo Cruz Foundation, Rio de Janeiro, Brazil. All leprosy patients were recruited with informed consent and approval from the Institutional Review Board of the University of California, Los Angeles, or the institutional ethics committee of Oswald Cruz Foundation.

Data availability

Data values reported in this manuscript are provided in the Supporting Data Values file. The sequencing data generated in this study are available on the NCBI GEO repository

database (GSE280021), along with additional datasets used for other analyses (GSE151528 and GSE125943).

Author Contributions

R.L.M. supervised and conceptualized the study. P.R.A. performed the experiments. F.M., J.L., P.R.A., and M.P. conducted the bioinformatics analysis. J.A., E.Y.L., and G.C.L.W. performed the machine learning classifier analysis. E.N.S. provided the leprosy skin lesions. J.E.G., C.D., D.M., R.M.B.T., B.J.A.S., G.A., L.A.M, J.P and B.B. provided methodological and analysis support. Funding was acquired by R.L.M. The manuscript was written by P.R.A. and R.L.M.

Acknowledgements

The funding sources for this work were: NIH grants R01 AI022553, R01 AR040312, R01 AR073252, R01 AI166313, R01 AI169526, P50 AR080594 and 4R37 AI052453-21, as well as NSF grant DMR2325840. Live *M. leprae* was kindly provided by the U.S. National Hansen's Disease Programs with financial support from NIAID AAI15006-004. The funders had no role in study design, data collection and analysis, decision to publish, or preparation of the manuscript. We gratefully acknowledge the UCLA Technology Center for Genomics & Bioinformatics (TCGB), the Advanced Light Microscopy and Spectroscopy (ALMS) Laboratory (CNSI), and the Electron Imaging Center for NanoMachines (EICN) (CNSI) for their invaluable assistance.

Figures and Legends

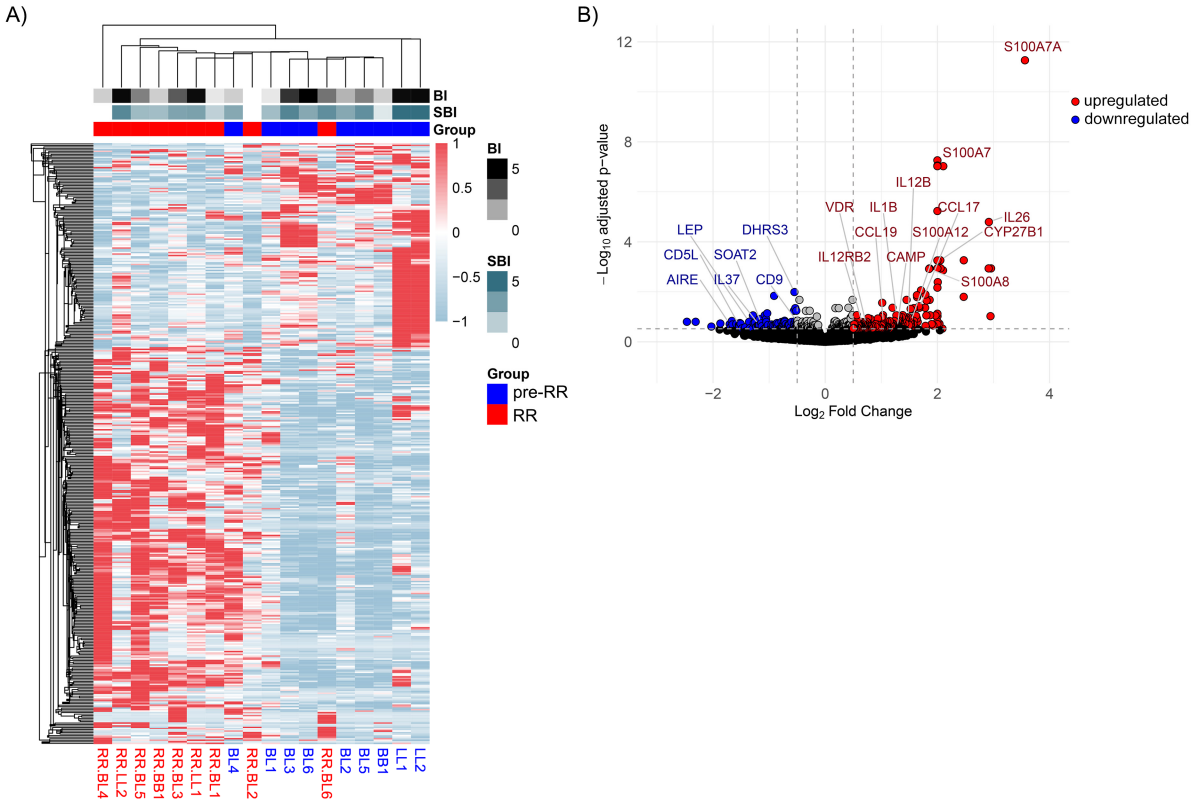

Figure 1: Differential gene expression analysis of RR vs. pre-RR groups. (**A**) Heatmap displaying expression z-scores of the 404 differentially expressed genes (*padj*<0.3) in RR vs. pre-RR specimens, representing high (red) and low expression levels (light blue). Samples were clustered using Euclidean distance and median linkage. (**B**) Volcano plot of the differential gene expression analysis showing RR upregulated genes (red) and downregulated genes (blue). Relevant genes were annotated in the plot.

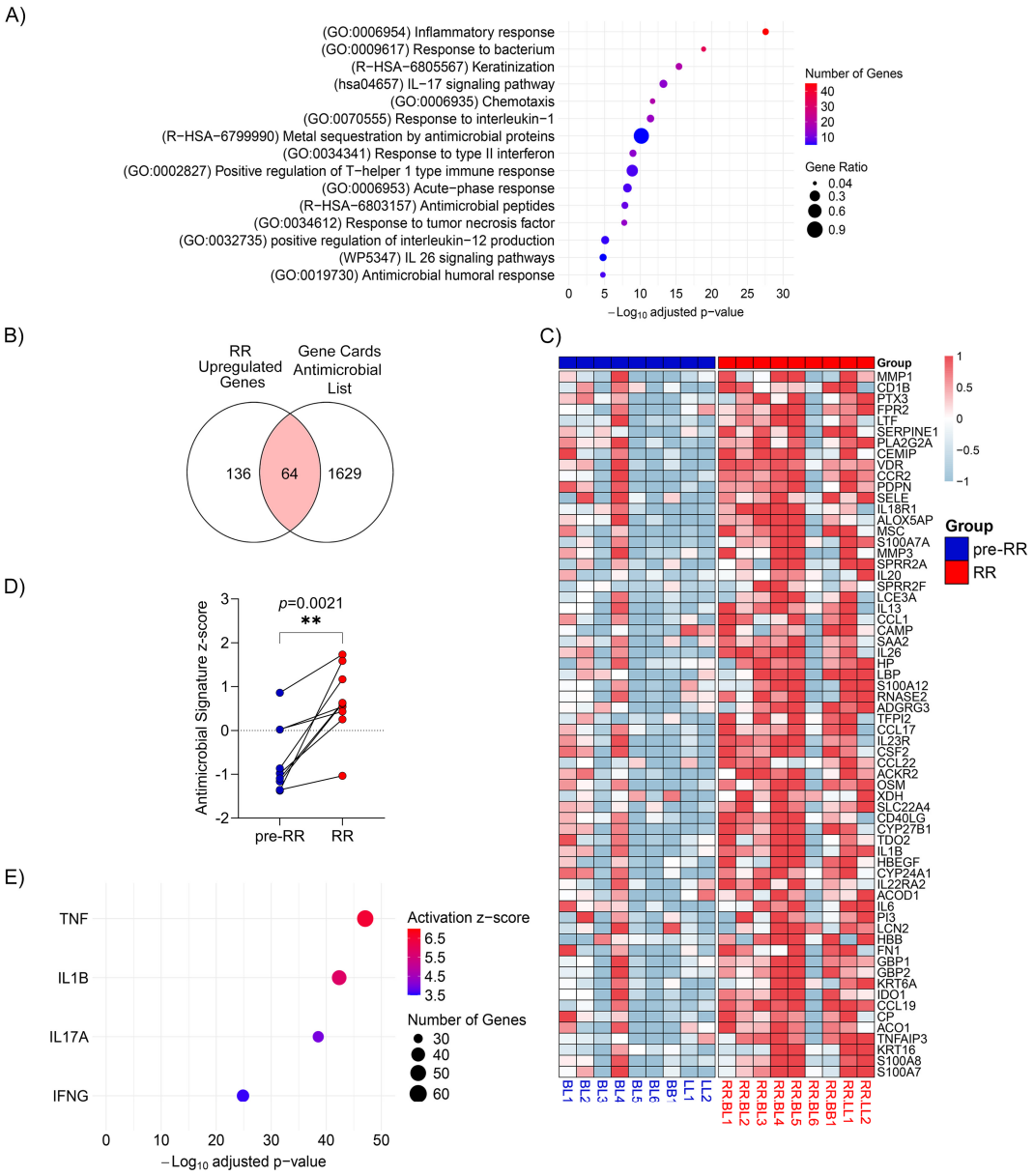

Figure 2: Functional analysis of RR upregulated genes. (**A**) Dot plot of selected host defense functional pathways enriched (-$\log_{10}$ *padj*>1.3 = *padj*<0.05) in the RR upregulated gene signature. (**B**) Venn diagram depicting overlap between the Gene Cards database antimicrobial gene signature (n=1,693) and the RR upregulated genes (n=200). (**C**) Heatmap displaying expression of 64 antimicrobial genes from each patient before (pre-RR) and at RR clinical onset (RR). (**D**) Antimicrobial response signature z-score of each patient before (pre-RR) and at RR clinical onset (RR). (**E**) Dot plot showing the UPR analysis of the 64 antimicrobial genes

upregulated in RR skin lesions performed by IPA. Statistical analyses were performed in GraphPad Prism 9.12 using the paired t test (**D**).

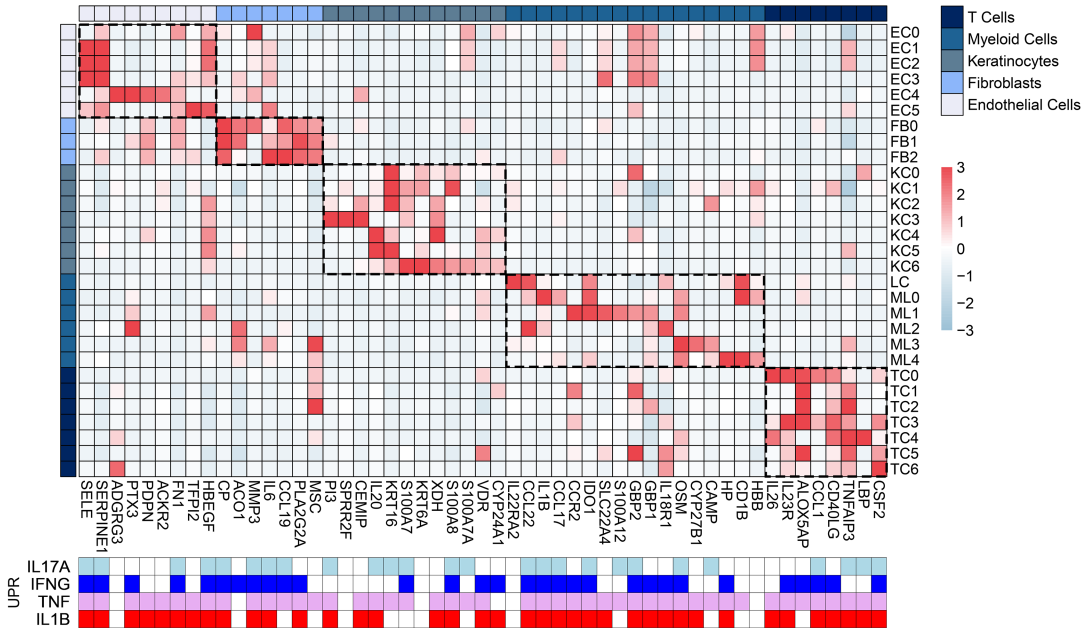

Figure 3: Different cell populations in RR skin lesions express the RR antimicrobial response signature. Heatmap of average expression z-scores of 53 out of the 64 genes from the RR antimicrobial response signature (z-score>2) detected in RR cell types defined by scRNA-seq (GSE151528). Heatmap's red to blue color scale indicates high to low expression. Cell type subclusters represent T cells (TC), Myeloid cells (LC and ML), Keratinocytes (KC), Fibroblasts (FB) and Endothelial cells (EC). The regulation of the antimicrobial genes (z-score>2) by their respective of upstream regulators (UPRs) is depicted as a heatmap at the bottom in light blue (*IL17A*), blue (*IFNG*) purple (*TNF*) and red (*IL1B*).

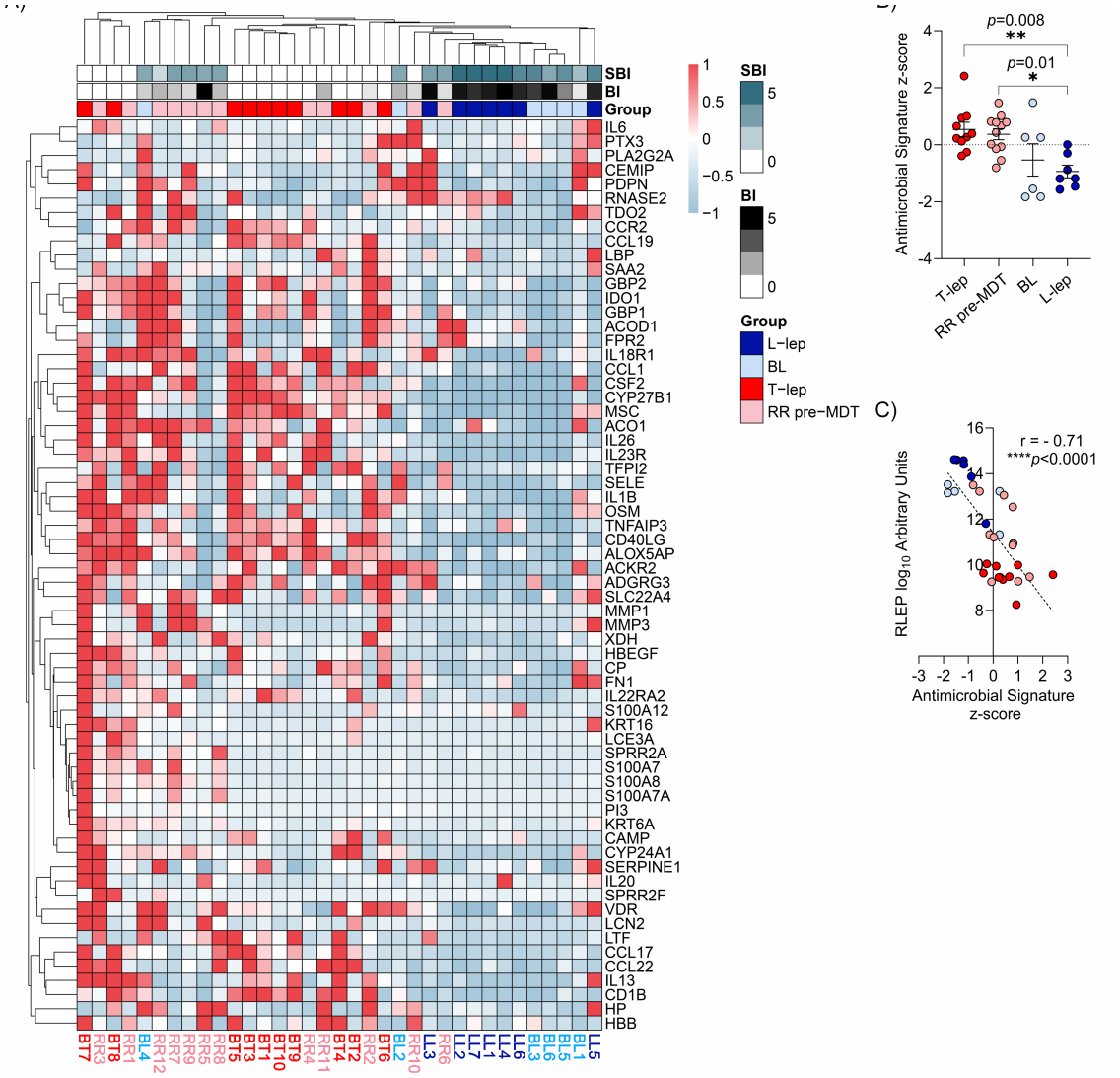

Figure 4: RR antimicrobial response signature is more expressed in T-lep and RR pre-MDT patients and negatively correlates with bacillary load. (**A**) Heatmap displaying expression z-scores of the 64 RR antimicrobial genes in leprosy clinical forms with red to light blue color scale indicating high to low expression. T-lep, RR pre-MDT, BL and L-lep samples were grouped by hierarchical clustering using Canberra distance and McQuitty linkage method. (**B**) Plot showing the antimicrobial response signature z-scores of each patient from T-lep (n=10), RR pre-MDT (n=12), BL (n=6) and L-lep (n=7) groups. Data represent the mean ± SEM. (**C**) Correlation analysis between *RLEP* expression and antimicrobial response gene signature z-scores of each patient from T-lep (red), RR pre-MDT (pink), BL (light blue) and L-lep (blue)

groups. Statistical analyses were performed in GraphPad Prism 9.12 using Ordinary One-way ANOVA test followed by Tukey's multiple comparisons test (**B**) and Spearman correlation coefficient (**C**).

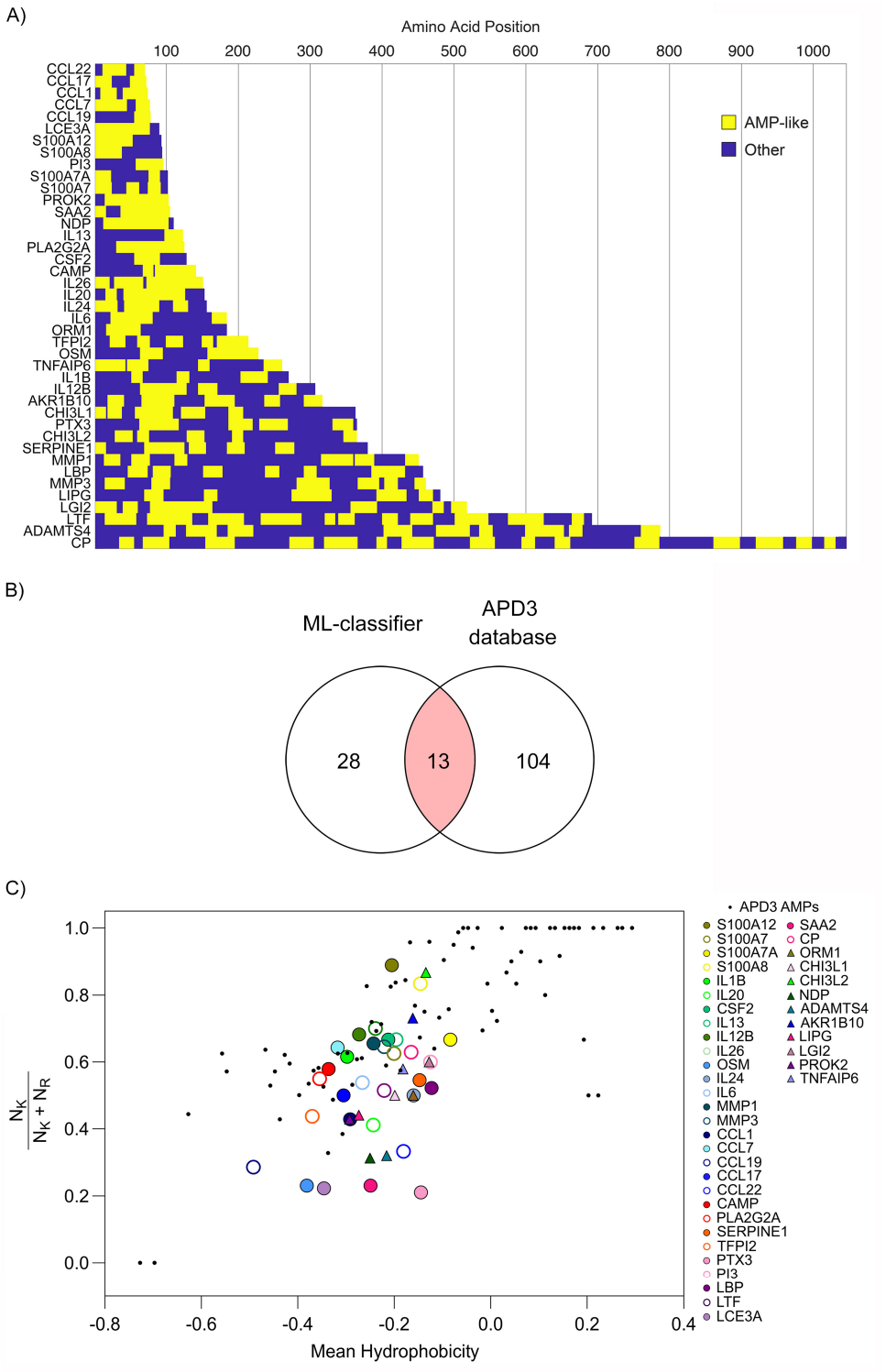

Figure 5: Genes upregulated in RR skin lesions encode proteins with membrane-active antimicrobial peptide motifs. (**A**) Graph displaying the amino acid position of the AMP-like motifs (yellow) identified along the protein sequence encoded by the RR upregulated genes. (**B**)

Venn diagram depicting the overlap between the 41 RR genes with AMP-like motifs and the human AMPs on the APD3 database (n=117). (**C**) Evaluation of cationic and hydrophobic content of the AMP-like motifs detected in 41 RR antimicrobial molecules (colored circles and triangles) shown in a plot of lysine (*K*) to arginine (*R*) ratio = $N_K/(N_K + N_R)$ vs. mean $\langle hydrophobicity \rangle$ together with known α-helical antimicrobial peptides from the APD3 database (black circles).

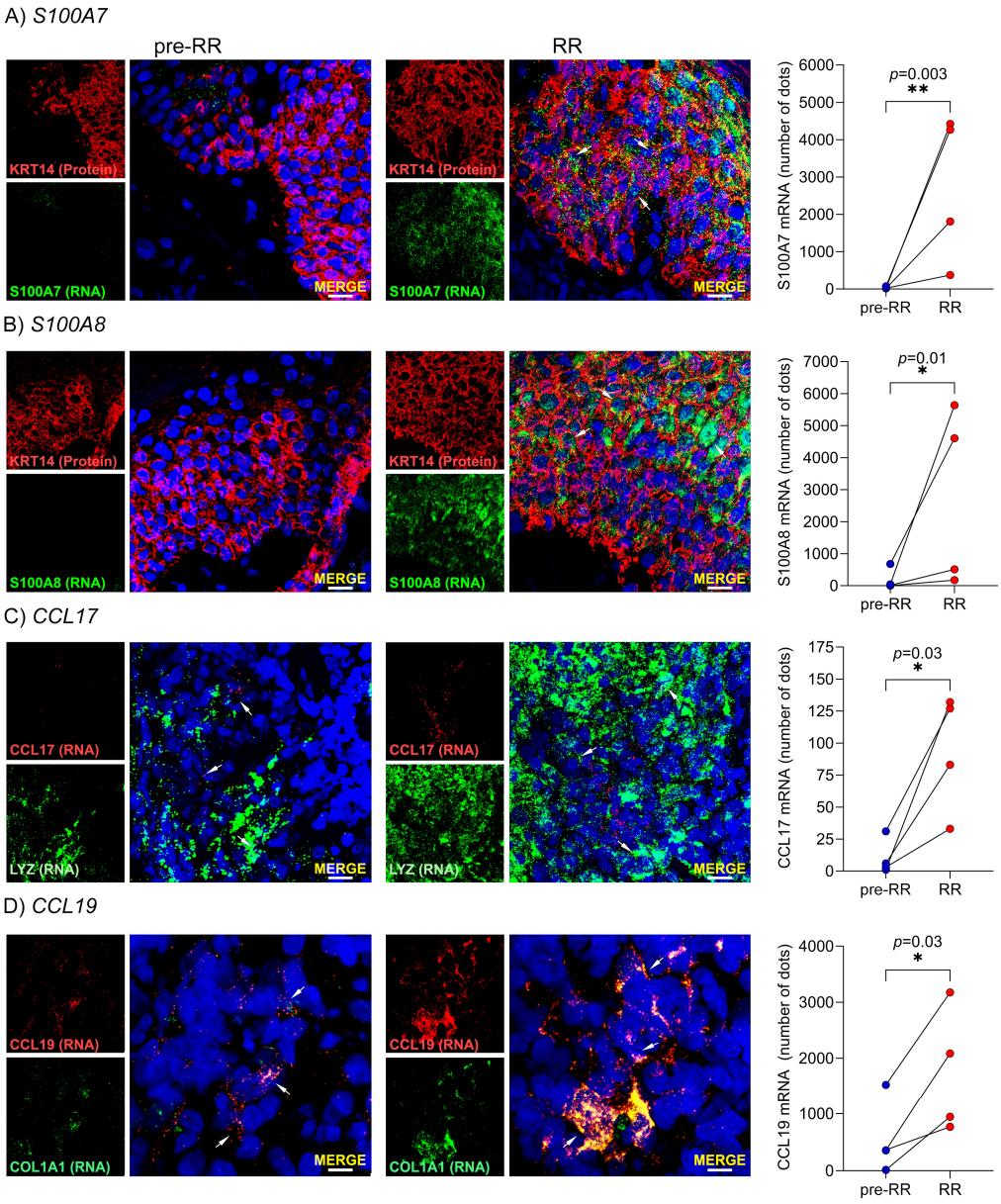

Figure 6: RNA-FISH shows antimicrobial gene expression in RR and pre-RR skin lesions by different cell populations. (**A**) RNA-FISH of *S100A7* (green) and protein staining of keratin 14 (KRT14) (red) in one representative pair of RR and pre-RR skin lesions (BL4/RR.BL4). Graph of *S100A7* RNA dot quantification (number of dots) performed on four pairs of RR and pre-RR skin lesions. (**B**) RNA-FISH of *S100A8* (green) and protein staining of KRT14 (red) in one representative pair of RR and pre-RR skin lesions (BL5/RR.BL5). Graph of *S100A8* RNA dot quantification (number of dots) performed on four pairs of RR and pre-RR skin lesions. (**C**)

RNA-FISH of *CCL17* (red) and *LYZ* (green), a macrophage marker, in one representative pair of RR and pre-RR skin lesions (BL3/RR.BL3). Graph of *CCL17* RNA dot quantification (number of dots) performed on four pairs of RR and pre-RR skin lesions. (**D**) RNA-FISH of *CCL19* (red) and *COL1A1* (green), a fibroblast marker, in one representative pair of RR and pre-RR skin lesions (BL4/RR.BL4). Graph of *CCL19* RNA dot quantification (number of dots) performed on four pairs of RR and pre-RR skin lesions. Cell nuclei were stained with DAPI (blue). Images were acquired with the Leica TCS SP8 Digital Light Sheet microscope and RNA dot quantification was performed using Image J. Scale bars = 10µm. Magnification = 630x (**A-C**) and 630x with 3x zoom (**D**). Statistical analyses were performed in GraphPad Prism 9.12 using ratio paired t test (**A and B**) or paired t test (**C and D**).

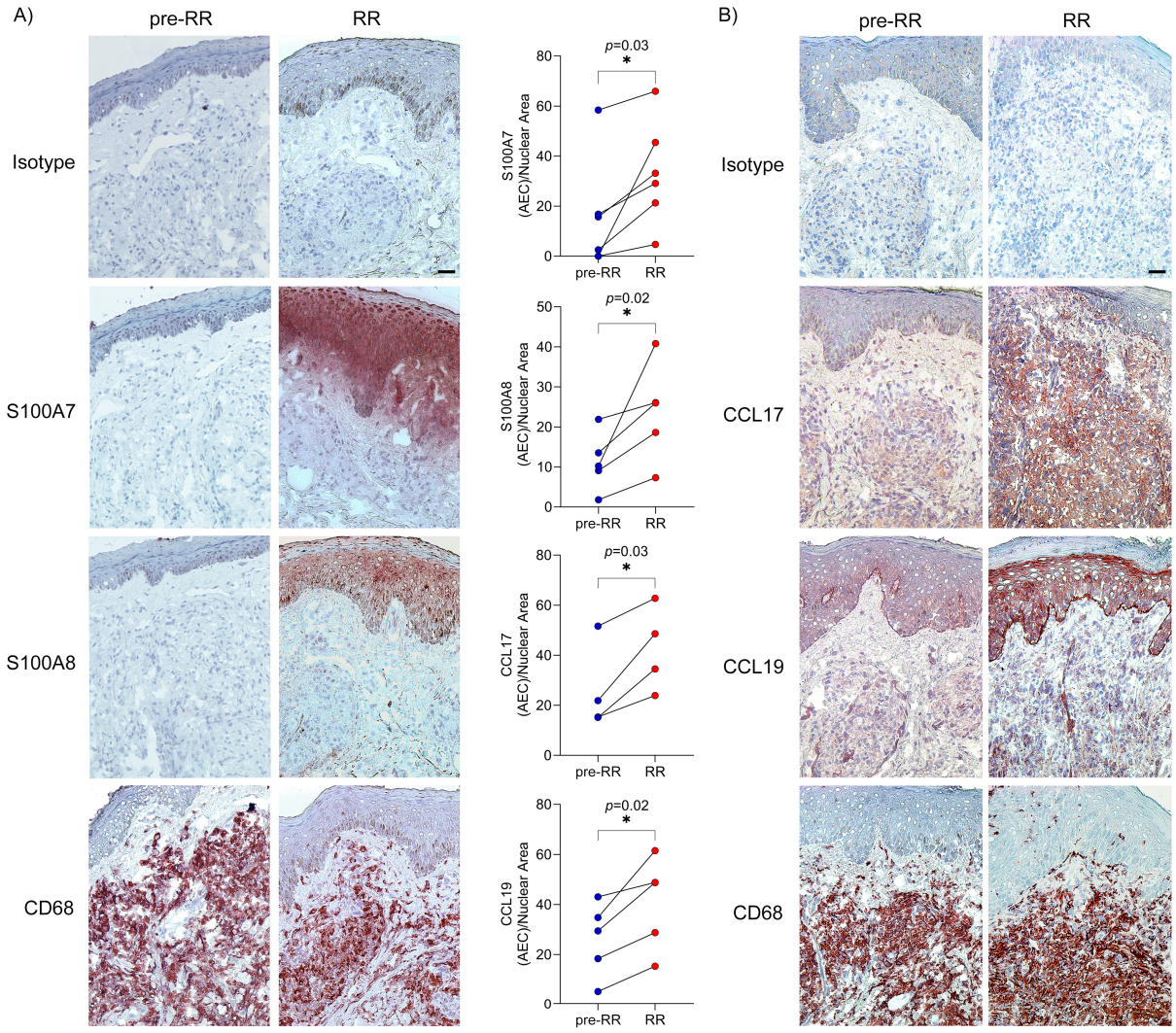

Figure 7: Protein expression of S100A7, S100A8, CCL17 and CCL19 in RR and pre-RR skin lesions. (**A**) S100A7 and S100A8 protein expression in a representative pre-RR and RR skin lesion pair (LL1/RR.LL1) evaluated by IHC. (**B**) CCL17 and CCL19 protein expression in a representative pre-RR and RR skin lesion pair (BL4/RR.BL4) evaluated by IHC. CD68, a macrophage marker, was used as a positive control. Graphs show quantification of S100A7 (n=6 pairs), S100A8 (n=5 pairs), CCL17 (n=4 pairs) and CCL19 (n=5 pairs) staining (AEC/nuclear area) by Image J plugin ImmunoRatio. Staining was visualized and images acquired using a Leica microscope (Leica 250). Scale bar = 25µm. Magnification = 200x.

Statistical analyses were performed in GraphPad Prism 9.12 using paired t test (**S100A7** and **CCL19**) or ratio paired t test (**S100A8** and **CCL17**).

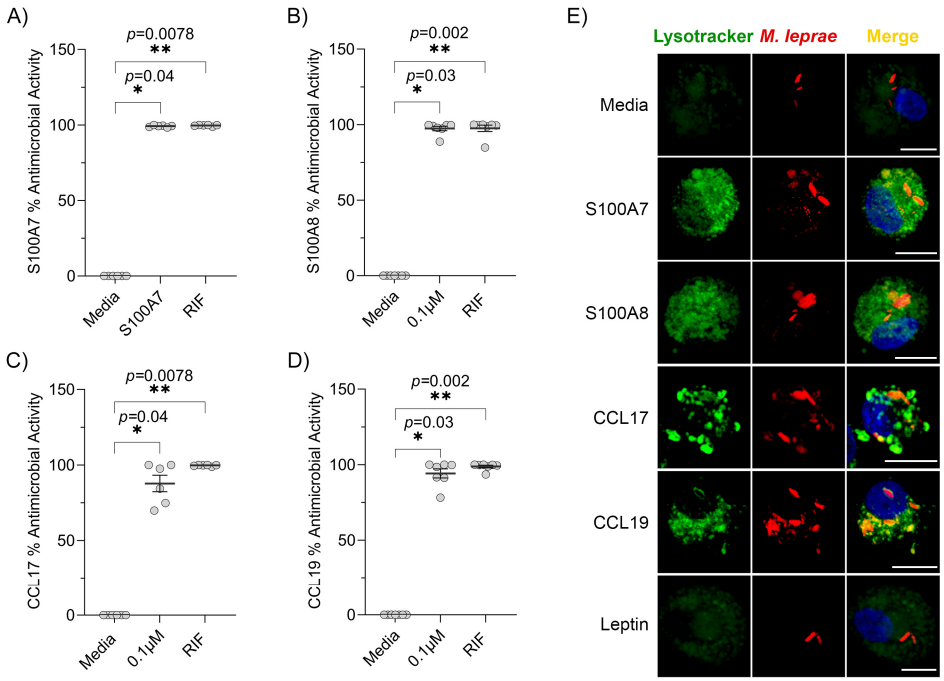

Figure 8: S100A7, S100A8, CCL17 and CCL19 exert antimicrobial activity against *M. leprae* in infected human macrophages. (**A-D**) MDMs from healthy donors were infected overnight with *M. leprae* at MOI of 5:1, followed by addition of 0.1µM of recombinant human S100A7, S100A8, CCL17 and CCL19 for 4 days. *M. leprae* viability was assessed by qPCR and percentage (%) antimicrobial activity was calculated by assigning 100% bacteria viability to the media control. Rifampin (10µg/ml) (RIF) was added as a positive control. (**E**) Lysosome acidification was evaluated by Lysotracker stanning (green) after 0.1µM recombinant human S100A7, S100A8, CCL17 and CCL19 stimulation in MDMs infected with *M. leprae* labeled with PKH26 (red) at MOI 5:1 for 24 hours. Leptin (0.1µM) was used as a negative control. Images were captured using a Leica TCS SP8 Digital Light Sheet Microscope. DAPI (blue) was used to stain the nuclei. Scale bar = 10µm, original magnification 630x with 4x zoom. Statistical analyses were performed in GraphPad Prism 9.12 using the Friedman test with Dunn's multiple comparisons test (**A-D**). Data represent the mean ± SEM (n=6 for **A** and **C**) and (n=7 **B** and **D**).

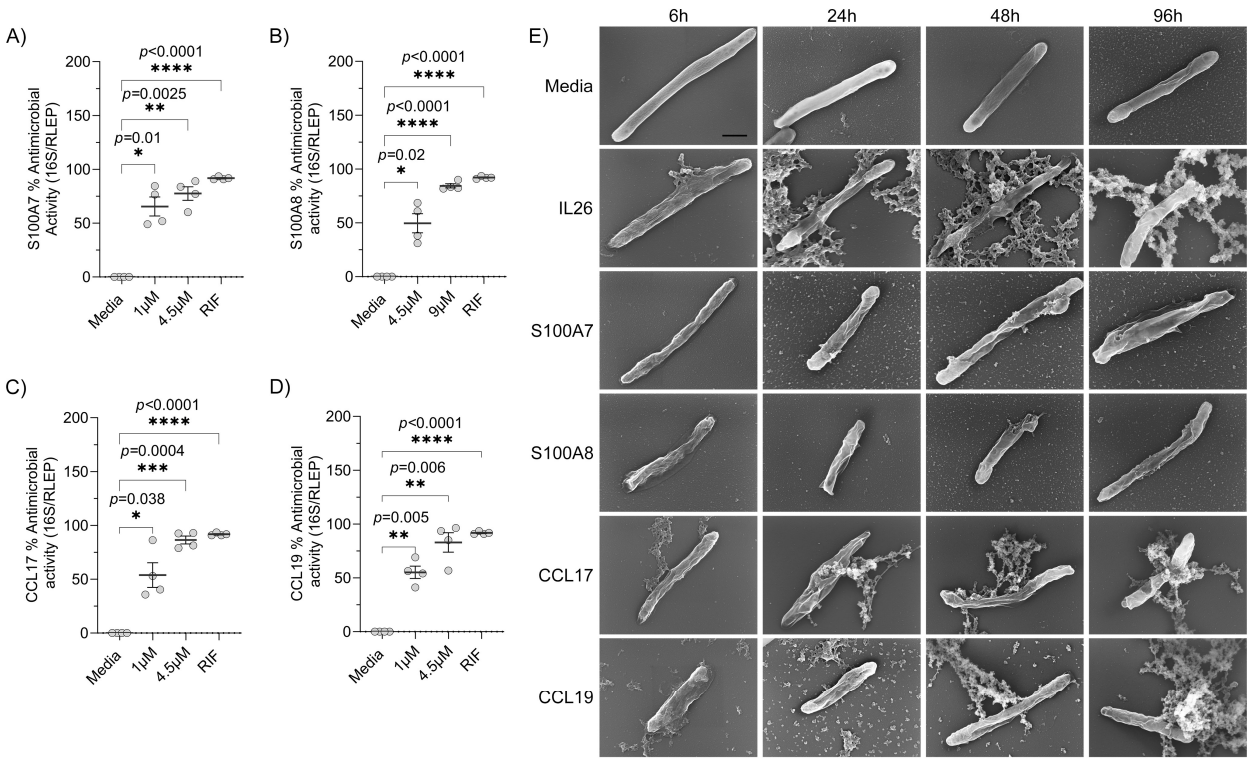

Figure 9: S100A7, S100A8, CCL17 and CCL19 exert direct antimicrobial activity against *M. leprae*. (**A-D**) Different concentrations of recombinant human S100A7, S100A8, CCL17 and CCL19 were added to *M. leprae* ($2x10^6$ bacilli) in 7H9 broth with 10mM sodium phosphate pH= 7.2 for 72 hours. Bacteria viability was assessed by qPCR and rifampin (10µg/ml) (RIF) was used as a positive control. (**E**) S100A7 (4.5µM), S100A8 (9µM), CCL17 (4.5µM) and CCL19 (4.5µM) were added to *M. leprae* ($15x10^6$ bacilli) in 7H9 broth with 10mM sodium phosphate pH=7.2 for 6, 24, 48 and 96 hours, and bacteria morphology was evaluated by scanning electron microscopy. IL26 (10µM) was used as a positive control. Magnification = 100,000X. Scale bar = 500nm. Statistical analyses performed in GraphPad Prism 9.12 using repeated measures ANOVA test with the Geisser-Greenhouse correction and Dunnett's multiple comparisons test (**A-D**). Data represent the mean ± SEM (n = 4).

References

1. Ridley DS, Jopling WH. Classification of leprosy according to immunity. A five-group system. *Int J Lepr Mycobact Dis Off Organ Int Lepr Assoc*. 1966;34(3):255–273.

2. Yamamura M, et al. Defining protective responses to pathogens: cytokine profiles in leprosy lesions. *Science*. 1991;254(5029):277–279.

3. Montoya D, et al. Divergence of macrophage phagocytic and antimicrobial programs in leprosy. *Cell Host Microbe*. 2009;6(4):343–353.

4. Teles RMB, et al. Type I interferon suppresses type II interferon-triggered human anti-mycobacterial responses. *Science*. 2013;339(6126):1448–1453.

5. Lienhardt C, Fine PE. Type 1 reaction, neuritis and disability in leprosy. What is the current epidemiological situation? *Lepr Rev*. 1994;65(1):9–33.

6. Walker SL, Lockwood DNJ. Leprosy type 1 (reversal) reactions and their management. *Lepr Rev*. 2008;79(4):372–386.

7. Nery JA da C, et al. Understanding the type 1 reactional state for early diagnosis and treatment: a way to avoid disability in leprosy. *An Bras Dermatol*. 2013;88(5):787–792.

8. Andrade PR, et al. Type 1 reaction in leprosy: a model for a better understanding of tissue immunity under an immunopathological condition. *Expert Rev Clin Immunol*. 2015;11(3):391–407.

9. Andrade PR, et al. CD123, the plasmacytoid dendritic cell phenotypic marker, is abundant in leprosy type 1 reaction. *Br J Dermatol*. 2015;172(1):268–271.

10. Cooper CL, et al. Analysis of naturally occurring delayed-type hypersensitivity reactions in leprosy by in situ hybridization. *J Exp Med*. 1989;169(5):1565–1581.

11. Waters MF, Turk JL, Wemambu SN. Mechanisms of reactions in leprosy. *Int J Lepr Mycobact Dis Off Organ Int Lepr Assoc*. 1971;39(2):417–428.

12. Modlin RL, et al. In situ characterization of T lymphocyte subsets in the reactional states of leprosy. *Clin Exp Immunol*. 1983;53(1):17–24.

13. Yamamura M, et al. Cytokine patterns of immunologically mediated tissue damage. *J Immunol Baltim Md 1950*. 1992;149(4):1470–1475.

14. Underhill DM, et al. Toll-like receptor-2 mediates mycobacteria-induced proinflammatory signaling in macrophages. *Proc Natl Acad Sci U S A*. 1999;96(25):14459–14463.

15. Krutzik SR, et al. IL-15 links TLR2/1-induced macrophage differentiation to the vitamin D-dependent antimicrobial pathway. *J Immunol Baltim Md 1950*. 2008;181(10):7115–7120.

16. Liu PT, et al. Toll-like receptor triggering of a vitamin D-mediated human antimicrobial response. *Science*. 2006;311(5768):1770–1773.

17. Liu PT, et al. Cutting edge: vitamin D-mediated human antimicrobial activity against Mycobacterium tuberculosis is dependent on the induction of cathelicidin. *J Immunol Baltim Md 1950*. 2007;179(4):2060–2063.

18. Ma F, et al. The cellular architecture of the antimicrobial response network in human leprosy granulomas. *Nat Immunol*. 2021;22(7):839–850.

19. Liu PT, et al. Convergence of IL-1beta and VDR activation pathways in human TLR2/1-induced antimicrobial responses. *PloS One*. 2009;4(6):e5810.

20. Realegeno S, et al. S100A12 Is Part of the Antimicrobial Network against Mycobacterium leprae in Human Macrophages. *PLoS Pathog*. 2016;12(6):e1005705.

21. Fabri M, et al. Vitamin D is required for IFN-gamma-mediated antimicrobial activity of human macrophages. *Sci Transl Med*. 2011;3(104):104ra102.

22. Silva BJ de A, et al. Autophagy Is an Innate Mechanism Associated with Leprosy Polarization. *PLoS Pathog*. 2017;13(1):e1006103.

23. Stenger S, et al. An antimicrobial activity of cytolytic T cells mediated by granulysin. *Science*. 1998;282(5386):121–125.

24. Balin SJ, et al. Human antimicrobial cytotoxic T lymphocytes, defined by NK receptors and antimicrobial proteins, kill intracellular bacteria. *Sci Immunol*. 2018;3(26):eaat7668.

25. Ernst WA, et al. Granulysin, a T cell product, kills bacteria by altering membrane permeability. *J Immunol Baltim Md 1950*. 2000;165(12):7102–7108.

26. Barman H, et al. Cholesterol in negatively charged lipid bilayers modulates the effect of the antimicrobial protein granulysin. *J Membr Biol*. 2006;212(1):29–39.

27. Dang AT, et al. IL-26 contributes to host defense against intracellular bacteria. *J Clin Invest*. 2019;129(5):1926–1939.

28. Meller S, et al. T(H)17 cells promote microbial killing and innate immune sensing of DNA via interleukin 26. *Nat Immunol*. 2015;16(9):970–979.

29. Hawerkamp HC, et al. Interleukin-26 activates macrophages and facilitates killing of Mycobacterium tuberculosis. *Sci Rep*. 2020;10(1):17178.

30. Barnetson RStC, et al. Does Nonspecific T-Lymphocyte Stimulation of B Lymphocytes Occur During Reversal Reaction in Borderline Leprosy? *Scand J Immunol*. 1976;5(3):287–292.

31. Roche PW, Theuvenet WJ, Britton WJ. Risk factors for type-1 reactions in borderline leprosy patients. *The Lancet*. 1991;338(8768):654–657.

32. Geluk A, et al. Longitudinal Immune Responses and Gene Expression Profiles in Type 1 Leprosy Reactions. *J Clin Immunol*. 2014;34(2):245–255.

33. Khadge S, et al. Longitudinal immune profiles in type 1 leprosy reactions in Bangladesh, Brazil, Ethiopia and Nepal. *BMC Infect Dis*. 2015;15:477.

34. Teles RMB, et al. Identification of a systemic interferon-γ inducible antimicrobial gene signature in leprosy patients undergoing reversal reaction. *PLoS Negl Trop Dis*. 2019;13(10):e0007764.

35. Tió-Coma M, et al. Whole blood RNA signatures in leprosy patients identify reversal reactions before clinical onset: a prospective, multicenter study. *Sci Rep*. 2019;9(1):17931.

36. Weiss DI, et al. IL-1β Induces the Rapid Secretion of the Antimicrobial Protein IL-26 from Th17 Cells. *J Immunol*. 2019;203(4):911–921.

37. Sieling PA, et al. IL-12 regulates T helper type 1 cytokine responses in human infectious disease. *J Immunol Baltim Md 1950*. 1994;153(8):3639–3647.

38. Nold MF, et al. IL-37 is a fundamental inhibitor of innate immunity. *Nat Immunol*. 2010;11(11):1014–1022.

39. Zhao B, et al. The Role of Autoimmune Regulator (AIRE) in Peripheral Tolerance. *J Immunol Res*. 2018;2018:3930750.

40. Tian J, et al. Hif1α/Dhrs3a Pathway Participates in Lipid Droplet Accumulation via Retinol and Ppar-γ in Fish Hepatocytes. *Int J Mol Sci*. 2023;24(12):10236.

41. Sun H-Y, et al. Sterol O-acyltransferase 2 chaperoned by apolipoprotein J facilitates hepatic lipid accumulation following viral and nutrient stresses. *Commun Biol*. 2021;4(1):1–14.

42. Sanchez-Moral L, et al. Multifaceted Roles of CD5L in Infectious and Sterile Inflammation. *Int J Mol Sci*. 2021;22(8):4076.

43. Huang W, Febbraio M, Silverstein RL. CD9 tetraspanin interacts with CD36 on the surface of macrophages: a possible regulatory influence on uptake of oxidized low density lipoprotein. *PloS One*. 2011;6(12):e29092.

44. Pereira S, et al. Tissue-Specific Effects of Leptin on Glucose and Lipid Metabolism. *Endocr Rev*. 2020;42(1):1–28.

45. Zhou Y, et al. Metascape provides a biologist-oriented resource for the analysis of systems-level datasets. *Nat Commun*. 2019;10(1):1523.

46. Hughes TK, et al. Second-Strand Synthesis-Based Massively Parallel scRNA-Seq Reveals Cellular States and Molecular Features of Human Inflammatory Skin Pathologies. *Immunity*. 2020;53(4):878-894.e7.

47. Liu Y, et al. The protective role of tissue-resident interleukin 17A-producing gamma delta T cells in Mycobacterium leprae infection. *Front Immunol*. 2022;13:961405.

48. Santos MB, et al. Distinct Roles of Th17 and Th1 Cells in Inflammatory Responses Associated with the Presentation of Paucibacillary Leprosy and Leprosy Reactions. *Scand J Immunol*. 2017;86(1):40–49.

49. Martinez AN, et al. Molecular determination of Mycobacterium leprae viability by use of real-time PCR. *J Clin Microbiol*. 2009;47(7):2124–2130.

50. Lee EY, et al. Mapping membrane activity in undiscovered peptide sequence space using machine learning. *Proc Natl Acad Sci*. 2016;113(48):13588–13593.

51. Wang G, Li X, Wang Z. APD3: the antimicrobial peptide database as a tool for research and education. *Nucleic Acids Res*. 2016;44(D1):D1087-1093.

52. Schmidt NW, et al. Criterion for Amino Acid Composition of Defensins and Antimicrobial Peptides Based on Geometry of Membrane Destabilization. *J Am Chem Soc*. 2011;133(17):6720–6727.

53. Keshav S, et al. Lysozyme is an inducible marker of macrophage activation in murine tissues as demonstrated by in situ hybridization. *J Exp Med*. 1991;174(5):1049–1058.

54. Andreu N, et al. Optimisation of Bioluminescent Reporters for Use with Mycobacteria. *PLOS ONE*. 2010;5(5):e10777.

55. Trindade MAB, et al. Granulomatous Reactivation during the Course of a Leprosy Infection: Reaction or Relapse. *PLoS Negl Trop Dis*. 2010;4(12):e921.

56. Saini C, Ramesh V, Nath I. CD4+ Th17 cells discriminate clinical types and constitute a third subset of non Th1, Non Th2 T cells in human leprosy. *PLoS Negl Trop Dis*. 2013;7(7):e2338.

57. Saini C, et al. Elevated IL-6R on CD4+ T cells promotes IL-6 driven Th17 cell responses in patients with T1R leprosy reactions. *Sci Rep*. 2020;10(1):15143.

58. Saini C, et al. Leprosy Reactions Show Increased Th17 Cell Activity and Reduced FOXP3+ Tregs with Concomitant Decrease in TGF-β and Increase in IL-6. *PLoS Negl Trop Dis*. 2016;10(4):e0004592.

59. Abdallah M, et al. Estimation of serum level of interleukin-17 and interleukin-4 in leprosy, towards more understanding of leprosy immunopathogenesis. *Indian J Dermatol Venereol Leprol*. 2013;79(6):772–776.

60. Chaitanya S, et al. Increased Serum Circulatory Levels of Interleukin 17F in Type 1 Reactions of Leprosy. *J Clin Immunol*. 2012;32(6):1415–1420.

61. Choudhary R, Chhabra N, Patel S. Comparison of Serum Levels of Interleukin 17 and Interleukin 9 in Leprosy Patients with and without Lepra Reaction: A Cross-Sectional Analytical Study from Central India. *Indian J Dermatol*. 2023;68(6):661.

62. Das M, et al. Mycobacterium leprae and host immune transcriptomic signatures for reactional states in leprosy. *Front Microbiol*. 2023;14. https://doi.org/10.3389/fmicb.2023.1113318.

63. Shanmugasundaram U, et al. Pulmonary Mycobacterium tuberculosis control associates with CXCR3- and CCR6-expressing antigen-specific Th1 and Th17 cell recruitment. *JCI Insight*. 2020;5(14):e137858, 137858.

64. Khader SA, et al. IL-23 and IL-17 in the establishment of protective pulmonary CD4+ T cell responses after vaccination and during Mycobacterium tuberculosis challenge. *Nat Immunol*. 2007;8(4):369–377.

65. Okamoto Yoshida Y, et al. Essential role of IL-17A in the formation of a mycobacterial infection-induced granuloma in the lung. *J Immunol Baltim Md 1950*. 2010;184(8):4414–4422.

66. Gideon HP, et al. Variability in tuberculosis granuloma T cell responses exists, but a balance of pro- and anti-inflammatory cytokines is associated with sterilization. *PLoS Pathog*. 2015;11(1):e1004603.

67. Schmidt NW, et al. Molecular basis for nanoscopic membrane curvature generation from quantum mechanical models and synthetic transporter sequences. *J Am Chem Soc*. 2012;134(46):19207–19216.

68. Zaia AA, et al. Subversion of antimicrobial calprotectin (S100A8/S100A9 complex) in the cytoplasm of TR146 epithelial cells after invasion by Listeria monocytogenes. *Mucosal Immunol*. 2009;2(1):43–53.

69. Clark HL, et al. Zinc and Manganese Chelation by Neutrophil S100A8/A9 (Calprotectin) Limits Extracellular Aspergillus fumigatus Hyphal Growth and Corneal Infection. *J Immunol Baltim Md 1950*. 2015;196(1):336.

70. Sohnle PG, Collins-Lech C, Wiessner JH. The zinc-reversible antimicrobial activity of neutrophil lysates and abscess fluid supernatants. *J Infect Dis*. 1991;164(1):137–142.

71. Murthy AR, et al. In vitro candidastatic properties of the human neutrophil calprotectin complex. *J Immunol Baltim Md 1950*. 1993;151(11):6291–6301.

72. Clohessy PA, Golden BE. Calprotectin-mediated zinc chelation as a biostatic mechanism in host defence. *Scand J Immunol*. 1995;42(5):551–556.

73. Nakashige TG, et al. Human calprotectin is an iron-sequestering host-defense protein. *Nat Chem Biol*. 2015;11(10):765–771.

74. Linge HM, et al. The human CXC chemokine granulocyte chemotactic protein 2 (GCP-2)/CXCL6 possesses membrane-disrupting properties and is antibacterial. *Antimicrob Agents Chemother*. 2008;52(7):2599–2607.

75. Hieshima K, et al. CCL28 Has Dual Roles in Mucosal Immunity as a Chemokine with Broad-Spectrum Antimicrobial Activity 1. *J Immunol*. 2003;170(3):1452–1461.

76. Egesten A, et al. SpeB of Streptococcus pyogenes differentially modulates antibacterial and receptor activating properties of human chemokines. *PloS One*. 2009;4(3):e4769.

77. Korndörfer IP, Brueckner F, Skerra A. The crystal structure of the human (S100A8/S100A9)2 heterotetramer, calprotectin, illustrates how conformational changes of interacting alpha-helices can determine specific association of two EF-hand proteins. *J Mol Biol*. 2007;370(5):887–898.

78. Dhiman R, et al. Interleukin 22 inhibits intracellular growth of Mycobacterium tuberculosis by enhancing calgranulin A expression. *J Infect Dis*. 2014;209(4):578–587.

79. Wang J, et al. MRP8/14 induces autophagy to eliminate intracellular Mycobacterium bovis BCG. *J Infect*. 2015;70(4):415–426.

80. Vogl T, et al. Mrp8 and Mrp14 are endogenous activators of Toll-like receptor 4, promoting lethal, endotoxin-induced shock. *Nat Med*. 2007;13(9):1042–1049.

81. Wolf R, et al. Chemotactic activity of S100A7 (Psoriasin) is mediated by the receptor for advanced glycation end products and potentiates inflammation with highly homologous but functionally distinct S100A15. *J Immunol Baltim Md 1950*. 2008;181(2):1499–1506.

82. Boyd JH, et al. S100A8 and S100A9 mediate endotoxin-induced cardiomyocyte dysfunction via the receptor for advanced glycation end products. *Circ Res*. 2008;102(10):1239–1246.

83. Ghavami S, et al. S100A8/A9 at low concentration promotes tumor cell growth via RAGE ligation and MAP kinase-dependent pathway. *J Leukoc Biol*. 2008;83(6):1484–1492.

84. Marcato LG, et al. The role of Toll-like receptors 2 and 4 on reactive oxygen species and nitric oxide production by macrophage cells stimulated with root canal pathogens. *Oral Microbiol Immunol*. 2008;23(5):353–359.

85. Tsoporis JN, et al. S100B interaction with the receptor for advanced glycation end products (RAGE): a novel receptor-mediated mechanism for myocyte apoptosis postinfarction. *Circ Res*. 2010;106(1):93–101.

86. Shubbar E, et al. Psoriasin (S100A7) increases the expression of ROS and VEGF and acts through RAGE to promote endothelial cell proliferation. *Breast Cancer Res Treat*. 2012;134(1):71–80.

87. Guglielmotto M, et al. AGEs/RAGE complex upregulates BACE1 via NF-κB pathway activation. *Neurobiol Aging*. 2012;33(1):196.e13–27.

88. Xu Y, et al. Harnessing of TLR-mediated autophagy to combat mycobacteria in macrophages. *Tuberculosis*. 2013;93:S33–S37.

89. Hou X, et al. Advanced glycation endproducts trigger autophagy in cadiomyocyte via RAGE/PI3K/AKT/mTOR pathway. *Cardiovasc Diabetol*. 2014;13:78.

90. Küper C, Beck F-X, Neuhofer W. Toll-like receptor 4 activates NF-κB and MAP kinase pathways to regulate expression of proinflammatory COX-2 in renal medullary collecting duct cells. *Am J Physiol Renal Physiol*. 2012;302(1):F38-46.

91. Zhang X, et al. Salivary Protein Panel to Diagnose Systolic Heart Failure. *Biomolecules*. 2019;9(12):766.

92. Kim J-W, et al. S100A8 in Serum, Urine, and Saliva as a Potential Biomarker for Systemic Lupus Erythematosus. *Front Immunol*. 2022;13. https://doi.org/10.3389/fimmu.2022.886209.

93. Niens M, et al. Serum chemokine levels in Hodgkin lymphoma patients: highly increased levels of CCL17 and CCL22. *Br J Haematol*. 2008;140(5):527–536.

94. Tveita A, et al. High Circulating Levels of the Homeostatic Chemokines CCL19 and CCL21 Predict Mortality and Disease Severity in COVID-19. *J Infect Dis*. 2022;226(12):2150.

95. Kamionka M. Engineering of Therapeutic Proteins Production in Escherichia coli. *Curr Pharm Biotechnol*. 2011;12(2):268–274.

96. Bhatwa A, et al. Challenges Associated With the Formation of Recombinant Protein Inclusion Bodies in Escherichia coli and Strategies to Address Them for Industrial Applications. *Front Bioeng Biotechnol*. 2021;9:630551.

97. Fontes ANB, et al. Genetic diversity of mycobacterium leprae isolates from Brazilian leprosy patients. *Lepr Rev*. 2009;80(3):302–315.

98. Gomes TA, et al. Genomic and Phenotypic Variations Among Thai-53 and Mycobacterium leprae Clinical Isolates: Implications for Leprosy Pathogenesis and Research. *Pathogens*. 2024;13(11):986.

99. Stefani MMA, et al. Whole genome sequencing distinguishes between relapse and reinfection in recurrent leprosy cases. *PLoS Negl Trop Dis*. 2017;11(6):e0005598.

100. Benjak A, et al. Phylogenomics and antimicrobial resistance of the leprosy bacillus Mycobacterium leprae. *Nat Commun*. 2018;9(1):352.

101. Montoya DJ, et al. Dual RNA-Seq of Human Leprosy Lesions Identifies Bacterial Determinants Linked to Host Immune Response. *Cell Rep*. 2019;26(13):3574-3585.e3.

102. Andrade PR, et al. The cell fate regulator NUPR1 is induced by Mycobacterium leprae via type I interferon in human leprosy. *PLoS Negl Trop Dis*. 2019;13(7):e0007589.

103. Pham TV, Jimenez CR. An accurate paired sample test for count data. *Bioinformatics*. 2012;28(18):i596–i602.

104. Ridley DS. A logarithmic index of bacilli in biopsies. 2. Evaluation. *Int J Lepr Mycobact Dis Off Organ Int Lepr Assoc*. 1967;35(2):187–193.

105. Ridley DS, Hilson GR. A logarithmic index of bacilli in biopsies. I. Method. *Int J Lepr Mycobact Dis Off Organ Int Lepr Assoc*. 1967;35(2):184–186.

106. Lee EY, et al. What can machine learning do for antimicrobial peptides, and what can antimicrobial peptides do for machine learning? *Interface Focus*. 2017;7(6):20160153.

107. Lee EY, Wong GCL, Ferguson AL. Machine learning-enabled discovery and design of membrane-active peptides. *Bioorg Med Chem*. 2018;26(10):2708–2718.

108. Tuominen VJ, et al. ImmunoRatio: a publicly available web application for quantitative image analysis of estrogen receptor (ER), progesterone receptor (PR), and Ki-67. *Breast Cancer Res BCR*. 2010;12(4):R56.

109. Lahiri R, Randhawa B, Krahenbuhl J. Application of a viability-staining method for Mycobacterium leprae derived from the athymic (nu/nu) mouse foot pad. *J Med Microbiol*. 2005;54(Pt 3):235–242.

110. Agak GW, et al. Extracellular traps released by antimicrobial T_H17 cells contribute to host defense. *J Clin Invest*. 2021;131(2). https://doi.org/10.1172/JCI141594.